



**UNIVERSIDAD DE INVESTIGACIÓN DE TECNOLOGÍA
EXPERIMENTAL YACHAY**

Escuela de Ciencias Físicas y Nanotecnología

**TÍTULO: Analysis of interannual climate variations over Ecuador
associated with the El Niño-Southern Oscillation (ENSO) using RegCM**

Trabajo de integración curricular presentado como requisito para la
obtención del título de Física

Autor:

Arianna Judith Paredes Quiñonez

Tutor:

PhD. Wladimir Banda Barragán

Cotutor:

PhD. Oscar Vinicio Chimborazo Guerrón

Urcuquí - Febrero 2025

AUTORÍA

Yo, **Paredes Quiñonez Arianna Judith**, con cedula de identidad 1150045035, declaro que las ideas, juicios, valoraciones, interpretaciones, consultas bibliográficas, definiciones y conceptualizaciones expuestas en el presente trabajo; así cómo, los procedimientos y herramientas utilizadas en la investigación, son de absoluta responsabilidad de el autor del trabajo de integracion curricular. Así mismo, me acojo a los reglamentos internos de la Universidad de Investigación de Tecnología Experimental Yachay.

Urcuquí, Febrero 2025

Arianna Judith Paredes Quiñonez

CI: 1150045035

AUTORIZACIÓN DE PUBLICACIÓN

Yo, **Paredes Quiñonez Arianna Judith**, con cedula de identidad 1150045035, cedo a la Universidad de Investigación de Tecnología Experimental Yachay, los derechos de publicación de la presente obra, sin que deba haber un reconocimiento económico por este concepto. Declaro además que el texto del presente trabajo de titulación no podrá ser cedido a ninguna empresa editorial para su publicación u otros fines, sin contar previamente con la autorización escrita de la Universidad.

Asimismo, autorizo a la Universidad que realice la digitalización y publicación de este trabajo de integración curricular en el repositorio virtual, de conformidad a lo dispuesto en el Art. 144 de la Ley Orgánica de Educación Superior.

Urcuquí, Febrero 2025

Arianna Judith Paredes Quiñonez

CI: 1150045035

DEDICATION

To my parents, whose love and wisdom are the root of all my achievements.

Arianna Judith Paredes Quiñonez

ACKNOWLEDGMENT

This work would not have been possible without the inspiration and mentorship of my advisors, Oscar Chimborazo and Wladimir Banda. I admire and appreciate their invaluable guidance, patience, and support throughout this research. I also have heartfelt gratitude to all the professors at Yachay Tech who taught me to love science and knowledge, despite any resistance on my part.

To my family, for supporting me in everything I pursue. To my mother, Mariana, who always has words of encouragement and a hot meal for me; to my father, Marlon, whose wise advice has shaped my character; and to my brother, Cristopher, who has been my constant guide through his example.

To my friends, for being both a source of laughter and inexhaustible knowledge. To Johan, for all the endless talks and his advice that I never follow; to Jhoao, for the cups of coffee in the middle of existential crises and the debates that we never let die; to Abimael, for being the cause and companion of the most incredible adventures of my life; to Damian, for making all the classes and endless study nights enjoyable; to Lenin, for your contagious good vibes that brighten up any situation; to Juan, for showing me the wonders of chaos in our conversations about everything and nothing. I am grateful to have crossed paths with such extraordinary individuals in this crazy world.

Finally, I would like to extend my gratitude to the Corporación Ecuatoriana para el Desarrollo de la Investigación y la Academia (CEDIA) for providing the High-Performance Computing (HPC) resources that were indispensable for the development of this study. I also wish to acknowledge the support provided by the Centro de Modelización Matemática en Áreas Clave para el Desarrollo (MODEMAT) at Escuela Politécnica Nacional, for the HPC resources utilized under the guidance of my supervisor, Oscar Chimborazo. Moreover, I sincerely thank the International Centre for Theoretical Physics (ICTP) for providing the RegCM5 model through their GitHub repository. The data and tools available from ICTP were essential in conducting the climate simulations required for this research. I am especially grateful to Graziano Giuliani from ICTP, who through his emails, provided invaluable assistance in resolving all my queries related to the use of the RegCM5 model. I also extend my appreciation to the Copernicus Climate Change Service for providing the ERA5 reanalysis data. The high-quality and comprehensive climate datasets played a pivotal role in the analysis and interpretation of the results presented herein.

The author of this thesis acknowledges the use of the following publicly-available software: for data analysis and visualization, the Python libraries Xarray¹, Matplotlib², MetPy³; and for improving text clarity, ChatGPT and Grammarly, which were only used to correct grammar and spelling errors in selected parts of the text.

Arianna Judith Paredes Quiñonez

Resumen

El fenómeno de El Niño-Oscilación del Sur es la fluctuación climática interanual más significativa, pues influye en la circulación atmosférica global y modifica los patrones meteorológicos. En este estudio se analizó su impacto en las variaciones climáticas en Ecuador mediante el sistema de modelado climático regional, versión 5.0.0, mediante simulaciones de alta resolución que abarcaron la compleja topografía ecuatoriana y la región de Niño uno y dos, esenciales para este análisis. Las condiciones de contorno provenientes del modelo de circulación general HadGEM2-ES, bajo un escenario de altas emisiones de gases de efecto invernadero, impulsaron las proyecciones de temperatura en superficie, precipitación total y otras variables relevantes. La validación se realizó comparando los resultados con datos reanalizados globales y aplicando corrección de sesgo mediante mapeo delta cuantílico, lo que mejoró significativamente la precisión de las proyecciones. Se identificaron eventos del fenómeno a partir de anomalías en la temperatura superficial y se analizaron proyecciones para el periodo 2021 a 2050, las cuales revelaron un calentamiento significativo en las zonas costeras y andinas, con incremento de precipitaciones durante eventos de El Niño y reducción en los de La Niña. Estos hallazgos contribuyen a una mejor comprensión de los impactos del fenómeno y apoyan el desarrollo de estrategias de adaptación y mitigación en Ecuador.

Palabras clave:

El Niño-Oscilación del Sur, modelado climático regional, corrección de sesgo, simulaciones de alta resolución, proyecciones climáticas

Abstract

The El Niño-Southern Oscillation phenomenon is the most significant interannual climatic fluctuation, influencing global atmospheric circulation and altering weather patterns. In this study, its impact on climatic variations in Ecuador was analyzed using the regional climate modeling system, version 5.0.0, through high-resolution simulations that captured Ecuador's complex topography and the Niño 1 and 2 region, which are essential for this analysis. Boundary conditions from the HadGEM2-ES general circulation model, under a high greenhouse gas emissions scenario, drove the projections for near-surface temperature, total precipitation, and other relevant variables. Validation was performed by comparing the results with global reanalysis data and applying bias correction using quantile delta mapping, significantly enhancing projection accuracy. Events of the phenomenon were identified based on anomalies in near-surface temperature, and projections for the period 2021 to 2050 revealed significant warming in coastal and Andean regions, with increased precipitation during El Niño events and decreased precipitation during La Niña events. These findings contribute to a better understanding of the phenomenon's impacts and support the development of adaptation and mitigation strategies in Ecuador.

Keywords:

El Niño-Southern Oscillation, regional climate modeling, bias correction, high-resolution simulations, climate projections

Contents

1	Introduction	1
1.1	ENSO Dynamics	1
1.2	Teleconnections	3
1.3	Predictability and Challenges	5
1.4	Research problem	7
1.5	Objectives	8
1.5.1	General objective	8
1.5.2	Specific objectives	8
2	Methodology	10
2.1	Software	10
2.1.1	RegCM5 Preprocessor	10
2.1.2	RegCM5 Simulation	12
2.2	Hardware	18
2.3	Data Analysis	18
2.3.1	Preprocessing Data	18
2.3.2	Model Validation	19
2.3.3	Bias Correction	21
2.3.4	Identification of El Niño and La Niña Events	23
2.3.5	Near-Future Projections	24
3	Results	25
3.1	Validation of the Present Simulation (1991-2020)	25
3.1.1	Near-Surface Air Temperature	25
3.1.2	Total Precipitation	27
3.1.3	Divergence of Winds at 10m	30
3.1.4	Divergence of Winds at 100m	32
3.1.5	Specific Humidity	34
3.1.6	Relative Humidity	37

3.2	Bias Correction	39
3.2.1	Near-Surface Air Temperature	39
3.2.2	Total Precipitation	42
3.3	Identification of El Niño and La Niña Events	45
3.4	Near-Future Projections	47
3.4.1	Near-Surface Air Temperature	47
3.4.2	Total Precipitation	48
4	Conclusions	51
	Bibliography	54

List of Figures

1.1	Schematic of atmospheric and oceanic conditions of ENSO in the tropical Pacific. Under normal conditions, the Walker Circulation features rising air and heavy rainfall over the warm western Pacific and descent over the cooler eastern Pacific, creating a "cold tongue" and a "warm pool" in sea surface temperatures. During El Niño, weakened trade winds shift the warm pool eastward, flatten the thermocline, and reduce upwelling, leading to a positive feedback loop of warming surface waters and weakening winds. La Niña intensifies trade winds, steepens the tilt of the thermocline, increases upwelling, and shifts the warm pool further west. Taken from "Introduction to El Niño Southern Oscillation in a Changing Climate" ⁴	2
1.2	Typical impacts of El Niño (top) and La Niña (bottom) on global weather patterns during the peak season of development in December–February. Taken from NOAA/Climate Prediction Center.	4
1.3	Floods in the city of Guayaquil (left) and La Camaronera (right) caused by the El Niño phenomenon, taken on February 19 and March 7 of 1998, respectively. Source: El Universo.	5
1.4	Illustration of a General Circulation Model (GCM) and a Regional Climate Model (RCM). GCMs simulate the climate system based on the fundamental laws of physics, chemistry, and biology, covering the entire globe. RCMs are specialized to simulate regional-scale climate processes more accurately by taking high-resolution factors into account, such as topography and coastlines. Taken from "The State of the Art and Fundamental Aspects of Regional Climate Modeling in South America" ⁵	6
2.1	Topography of the simulation domain for both the present and near-future period. The red square encloses the continental region of Ecuador. The orange square encloses the Galapagos Islands, and the yellow square encloses the El Niño 1+2 region. These three squares conform to our target area of study.	11

3.1	Annual mean near-surface air temperature from RegCM5 simulation (left), ERA5 reanalysis data (middle), and the bias between them (right) for the period 1991-2020. The bias map highlights areas where the RegCM5 simulation overestimates temperatures, particularly along the Pacific coast, the Andes highlands, and the Insular region (shown in red), and areas where it underestimates temperatures, such as parts of the Amazon basin and some regions within the Andes (shown in blue).	26
3.2	Composite near-surface air temperature for El Niño (top row) and La Niña (bottom row) events from RegCM5 simulation (left), ERA5 reanalysis data (middle), and the bias between them (right) for the period 1991-2020. During El Niño events, RegCM5 simulation overestimates temperatures along the Pacific coast and in the insular region (shown in red), while underestimating temperatures within the Andean and Amazon regions (shown in blue). During La Niña events, the model overestimates temperatures in the highlands of the Andes, as well as in some areas of the coastal and insular regions (shown in red), while underestimating temperatures within the Andes and Amazon areas (shown in blue).	26
3.3	Annual mean total precipitation from RegCM5 simulation (left), ERA5 reanalysis data (middle), and the bias between them (right) for the period 1991-2020. The bias map highlights that the RegCM5 simulation overestimates precipitation in the central Andean region and the Amazon basin (shown in red), while it underestimates precipitation along the coastal region (shown in blue).	28
3.4	Composite total precipitation for El Niño (top row) and La Niña (bottom row) events from RegCM5 simulation (left), ERA5 reanalysis data (middle), and the bias between RegCM5 and ERA5 (right) for the period 1991-2020. During El Niño events, RegCM5 simulation overestimates precipitation in the Andean region and in some areas of the Amazon basin (shown in red), while underestimating the temperature along the Pacific coast (shown in blue). During La Niña events, the model continues to overestimate precipitation in the Andean and Amazon region, but also in some coastal areas (shown in red), while underestimating it in other coastal areas (shown in blue).	28
3.5	Annual mean wind divergence at 10m from RegCM5 simulation (left), ERA5 reanalysis data (middle), and the bias between them (right) for the period 1991-2020. The divergence is shown in 1/s and the arrows represent the direction and velocity of the winds. The bias map highlights areas where the RegCM5 simulation overestimates divergence, particularly in some areas of the coastal and Amazon regions (shown in red), and areas where it underestimates divergence, such as the Andean region (shown in blue).	30

3.6 Composite wind divergence at 10m for El Niño (top row) and La Niña (bottom row) events from RegCM5 simulation (left), ERA5 reanalysis data (middle), and the bias between them (right) for the period 1991-2020. The divergence is shown in 1/s and the arrows represent the direction and velocity of the winds. During El Niño events, the RegCM5 simulation overestimates divergence along the coast and Amazon regions (shown in red), while underestimating it in the Andean region (shown in blue). During La Niña events, the model shows similar discrepancies. 31

3.7 Annual mean wind divergence at 100m from RegCM5 simulation (left), ERA5 reanalysis data (middle), and the bias between them (right) for the period 1991-2020. The divergence is shown in 1/s and the arrows represent the direction and velocity of the winds. The bias map highlights areas where the RegCM5 simulation overestimates divergence, particularly along the coastal regions and parts of the Amazon basin (shown in red), and areas where it underestimates divergence, such as the Andean region (shown in blue). 32

3.8 Composite wind divergence at 100m for El Niño (top row) and La Niña (bottom row) events from RegCM5 simulation (left), ERA5 reanalysis data (middle), and the bias between them (right) for the period 1991-2020. The divergence is shown in 1/s and the arrows represent the direction and velocity of the winds. During El Niño events, the RegCM5 simulation overestimates divergence in the coastal and Amazon regions (shown in red), while underestimating it in the Andean region (shown in blue). During La Niña events, the model shows similar discrepancies. 33

3.9 Annual mean specific humidity from RegCM5 simulation (left), ERA5 reanalysis data (middle), and the bias between them (right) for the period 1991-2020. The bias map highlights areas where the RegCM5 simulation underestimates specific humidity, particularly in the Amazon region, along the coast, and in the insular region (shown in blue), and areas where it overestimates specific humidity, such as the Andean region (shown in red). 35

3.10 Composite specific humidity for El Niño (top row) and La Niña (bottom row) events from RegCM5 simulation (left), ERA5 reanalysis data (middle), and the bias between them (right) for the period 1991-2020. During El Niño events, the RegCM5 simulation underestimates specific humidity in the Amazon region, along the coast, and in the insular region (shown in blue), while overestimating it in the Andean region (shown in red). During La Niña events, the model shows similar discrepancies but with less magnitude. 35

3.11 Annual mean relative humidity from RegCM5 simulation (left), ERA5 reanalysis data (middle), and the bias between them (right) for the period 1991-2020. The bias map shows that the RegCM5 simulation underestimates relative humidity along the coast and some parts of the Amazon region (shown in blue) while overestimating it in the Andean region (shown in red). 37

3.12 Composite relative humidity for El Niño (top row) and La Niña (bottom row) events from RegCM5 simulation (left), ERA5 reanalysis data (middle), and the bias between them (right) for the period 1991-2020. During El Niño events, RegCM5 simulation generally underestimates relative humidity in coastal and Amazon regions (shown in blue), while overestimating it in the Andean region (shown in red). During La Niña events, the model shows very similar discrepancies. 38

3.13 Annual mean near-surface air temperature from RegCM5 simulation with bias correction (left), ERA5 reanalysis data (middle), and the bias between them (right) for the period 2011-2020. The bias map highlights areas where the RegCM5 simulation underestimates temperatures, particularly throughout continental Ecuador (shown in blue). 39

3.14 Composite near-surface air temperature for El Niño (top row) and La Niña (bottom row) events from RegCM5 simulation with bias correction (left), ERA5 reanalysis data (middle), and the bias between them (right) for the period 2011-2020. During El Niño events, RegCM5 simulation underestimates temperatures along the Pacific coast, the insular, and Andean region (shown in blue), while overestimating temperatures in some areas of the Amazon basin (shown in red). During La Niña events, the model overestimates temperatures in the Andes, as well as in some areas of the Amazon region (shown in red), while underestimating temperatures in some coast areas (shown in blue). 40

3.15 Annual Cycle of near-surface air temperature for the period 2011-2020. The bias-corrected model (RegCM5_QDM) aligns more closely with ERA5 data, particularly during the cooler months from July to December, reducing the overall error and improving the representation of seasonal temperature variations in Ecuador. 41

3.16 Annual mean precipitation from RegCM5 simulation data corrected (left), ERA5 reanalysis data (middle), and the bias between them (right) for the period 2011-2020. The bias map highlights areas where the RegCM5 simulation overestimates precipitation, particularly along the Pacific coast and some areas of the Andean region (shown in red), while overestimating precipitation in the Amazon region (shown in blue). 42

3.17	Composite precipitation for El Niño (top row) and La Niña (bottom row) events from RegCM5 simulation data corrected (left), ERA5 reanalysis data (middle), and the bias between them (right) for the period 2011-2020. During El Niño events, RegCM5 simulation underestimates precipitations along the Pacific coast and in the Amazon basin (shown in blue). During La Niña events, the model overestimates precipitations in the coast region, as well as in some areas of the Andean region (shown in red), while underestimating temperatures in the Amazon basin (shown in blue).	43
3.18	Annual Cycle of total precipitation for the period 2011-2020. The original model (RegCM5) consistently overestimates precipitation throughout the year compared to ERA5 data, with a pronounced peak during the wet season. The corrected model (RegCM5_QDM) aligns much more closely with ERA5. This alignment reduces the overall error and provides a more accurate representation of the seasonal precipitation variation in Ecuador.	44
3.19	Three-month running mean of the Sea Surface Temperature of the El Niño 1+2 Region for the period 1991-2020	45
3.20	Near-surface air temperature for the near future (2021-2050) and present period (1991-2020) with their respective projection. The left panel shows the mean temperature for the near-future period, indicating higher temperatures compared to the present period shown in the middle panel. The projection in the right panel highlights an overall increase in temperature, with the most pronounced warming observed in the Amazon and Andean regions.	47
3.21	Composite near-surface air temperature for El Niño and La Niña events in the near future (2021-2050) compared to the present period (1991-2020). The top row shows El Niño events, indicating a noticeable increase in temperature in the near future, particularly over the Pacific Ocean. The bottom row presents La Niña events, with a significant warming observed in the near future, especially in the Andean region. . .	48
3.22	Total precipitation for the near future (2021-2050) and present period (1991-2020) with their respective projections. The left panel shows the mean precipitation for the near-future period, indicating changes in precipitation patterns across the region compared to the present period shown in the middle panel. The projection in the right panel highlights areas of increased precipitation, particularly in the coastal and Andean regions.	49

3.23 Composite total precipitation for El Niño and La Niña events in the near future (2021-2050) compared to the present period (1991-2020). The top row shows El Niño events, indicating a significant increase in precipitation in the near future, particularly along the Pacific coast and parts of the Andean regions. The bottom row presents La Niña events, with a noticeable decrease in precipitation in the near future, especially in the Pacific coast and the Andean region. 49

Chapter 1

Introduction

The El Niño-Southern Oscillation (ENSO) is recognized as the most significant interannual climate fluctuation influencing global atmospheric circulation, thereby affecting weather and climate patterns worldwide⁶. ENSO comprises irregular periods of warming (El Niño) and cooling (La Niña) in the surface waters of the tropical eastern Pacific Ocean, driven by complex interactions between sea surface temperatures (SST) and atmospheric conditions in the equatorial Pacific⁴. During El Niño events, weakened trade winds reduce the upwelling of colder, nutrient-rich water off the coast of South America, leading to increased SSTs in the central and eastern tropical Pacific. Conversely, La Niña events are marked by stronger-than-usual trade winds and enhanced upwelling, resulting in colder SSTs⁷. The neutral phase is characterized by a balance in the tropical Pacific climate system without the significant deviations seen in El Niño or La Niña events⁸. Figure 1 provides a schematic representation of these phases, illustrating the distinct atmospheric and oceanic conditions.

ENSO is a very unpredictable phenomenon since it shows variations in intensity, frequency, and duration. Each phase can last from a few months to a year⁹. This phenomenon greatly influences the global atmospheric circulation, as it alters the position and intensity of the jet stream and the trajectories of storms in the Pacific. The jet stream is a band of fast-moving winds that moves from west to east in the upper atmosphere, significantly influencing weather and climate patterns. Therefore, these changes can lead to extreme weather events with environmental and socioeconomic impacts around the world¹⁰.

1.1 ENSO Dynamics

The dynamics of ENSO involve intricate interactions between the atmosphere and the ocean, primarily driven by feedback mechanisms like the **Bjerknes** and **thermocline** feedbacks. The Bjerknes feedback, identified by Jacob Bjerknes, links SSTs in the eastern tropical Pacific with overlying atmospheric

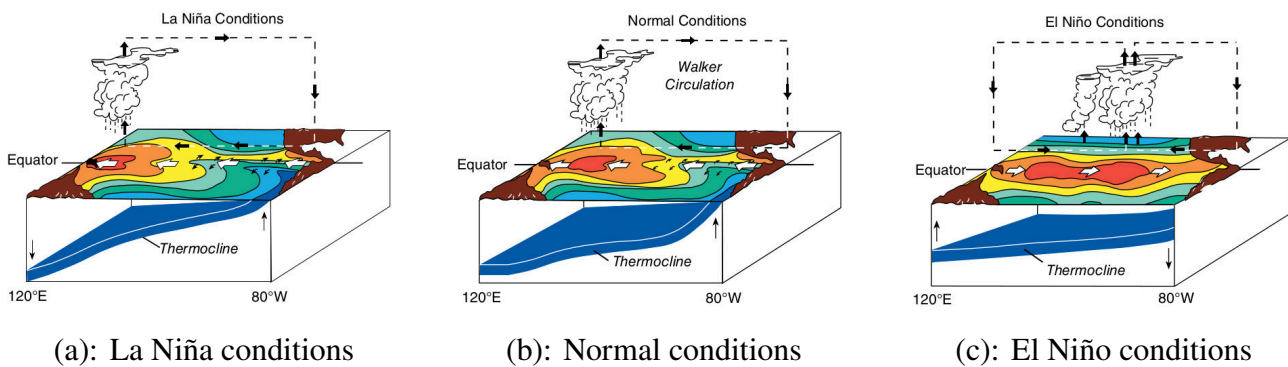


Figure 1.1: Schematic of atmospheric and oceanic conditions of ENSO in the tropical Pacific. Under normal conditions, the Walker Circulation features rising air and heavy rainfall over the warm western Pacific and descent over the cooler eastern Pacific, creating a "cold tongue" and a "warm pool" in sea surface temperatures. During El Niño, weakened trade winds shift the warm pool eastward, flatten the thermocline, and reduce upwelling, leading to a positive feedback loop of warming surface waters and weakening winds. La Niña intensifies trade winds, steepens the tilt of the thermocline, increases upwelling, and shifts the warm pool further west. Taken from "Introduction to El Niño Southern Oscillation in a Changing Climate"⁴.

conditions, wherein a reduction in the east-west temperature gradient weakens trade winds, reducing upwelling and allowing warmer waters to propagate eastward, amplifying the initial warming¹¹. The thermocline, a layer in the ocean where the temperature gradient is most pronounced, also plays a crucial role in ENSO dynamics. During El Niño, the thermocline depth decreases in the eastern Pacific, reducing the cooling effect of upwelling, thereby reinforcing the warming. During La Niña, the deeper thermocline in the eastern Pacific promotes the upwelling of cooler waters, sustaining or strengthening the cooling¹².

Extending this understanding, the **Zebiak-Cane model**, a pivotal coupled ocean-atmosphere model, provides deeper insights into the propagation of oceanic waves and their role in ENSO events¹³. This model elucidates how Kelvin and Rossby waves contribute significantly to the development and decay of ENSO phenomena. Wind anomalies in the western Pacific initiate Kelvin waves. These waves travel eastward along the equator, causing a deepening of the thermocline. As these Kelvin waves move eastward, they spread warm water across the Pacific, diminishing the cooling effect produced by upwelling cold water from the deeper ocean layers¹⁴. This deepening of the thermocline in the eastern Pacific reduces the efficiency of upwelling to cool the surface waters, thereby reinforcing the warming associated with El Niño events. This mechanism amplifies the initial warming signal and sustains the El Niño conditions. On the other hand, Rossby waves propagate westward, playing a crucial role in the termination of El Niño events. As these waves move westward, triggered by the changes in wind patterns, they induce a rise in the thermocline in the western Pacific. This elevation of the thermocline restores the normal upwelling of cooler, nutrient-rich waters, which helps to cool the

SSTs. Reestablishing these conditions contributes to the transition from El Niño to La Niña or neutral phases¹⁵. Thus, Rossby waves facilitate the decay of El Niño events by restoring the thermocline of the equatorial Pacific to its pre-El Niño state.

1.2 Teleconnections

The impacts of ENSO extend beyond the Pacific region through atmospheric teleconnections, influencing global weather patterns and climate conditions. Changes in SST and atmospheric circulation in the equatorial Pacific can affect phenomena such as the Indian monsoon, North Atlantic storm tracks, and rainfall patterns in the Americas and Africa. El Niño typically increases precipitation in the southern United States and Peru, causing floods and landslides, while regions like Indonesia, the Philippines, and northeastern Australia often experience droughts. La Niña generally produces opposite effects, promoting dry conditions in the southern United States and increased rainfall in Southeast Asia and Australia¹⁶. Moreover, ENSO influences global temperatures, with El Niño episodes generally leading to higher global temperatures due to the redistribution of warm ocean water, particularly affecting the tropics and subtropics. La Niña episodes, in contrast, are associated with cooler global temperatures. The alteration of normal weather patterns during ENSO phases can lead to extreme weather events, such as fewer hurricanes in the Atlantic and more cyclones in the Pacific during El Niño, and the opposite during La Niña¹⁷.

In South America, the teleconnections of ENSO have substantial regional climate impacts. El Niño events often lead to increased rainfall on the northern coast of Peru and Ecuador, causing severe flooding and landslides. Conversely, the Amazon Basin typically experiences decreased precipitation during these events, exacerbating drought conditions and affecting water availability and agriculture. In contrast, La Niña usually brings drier weather to the coastal regions of Peru and Ecuador while enhancing rainfall in southeastern Brazil and the Andean highlands, influencing water resources and agricultural productivity^{18 19}.

For Ecuador, ENSO teleconnections have significant impacts on the climate, particularly in the coastal and Andean regions. During El Niño events, the warming of sea surface temperatures in the eastern Pacific leads to enhanced convection and increased rainfall along the Pacific coast. This results in frequent and intense rainfall episodes, causing severe flooding, landslides, and infrastructure damage²⁰. The coastal provinces, such as Guayas, Manabí, and Esmeraldas, are particularly vulnerable to these effects. This alters the hydrological cycle, affecting water resources that are crucial for hydropower generation and irrigation²¹.

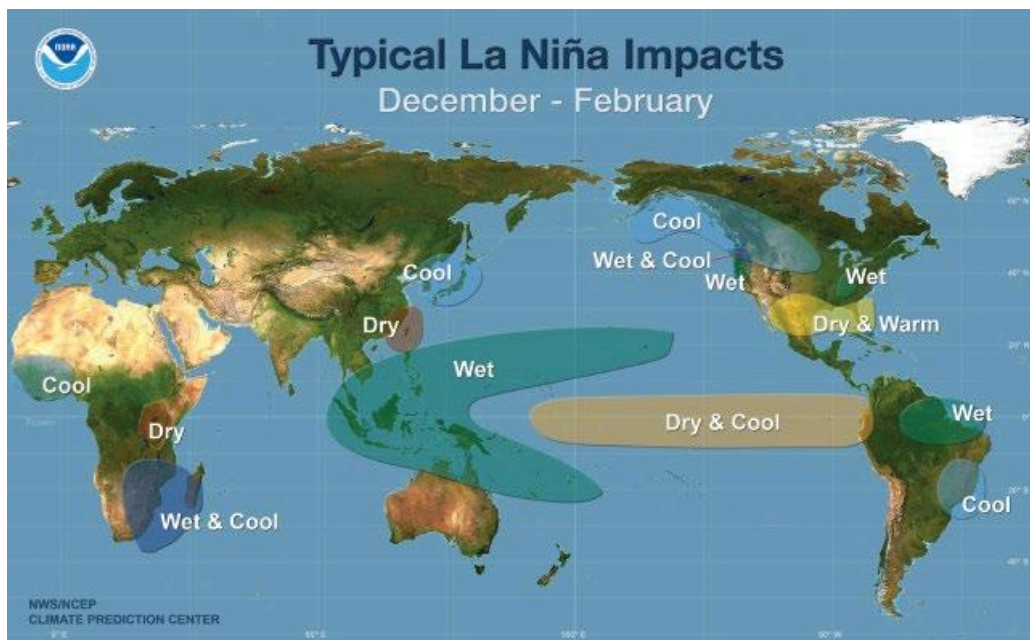
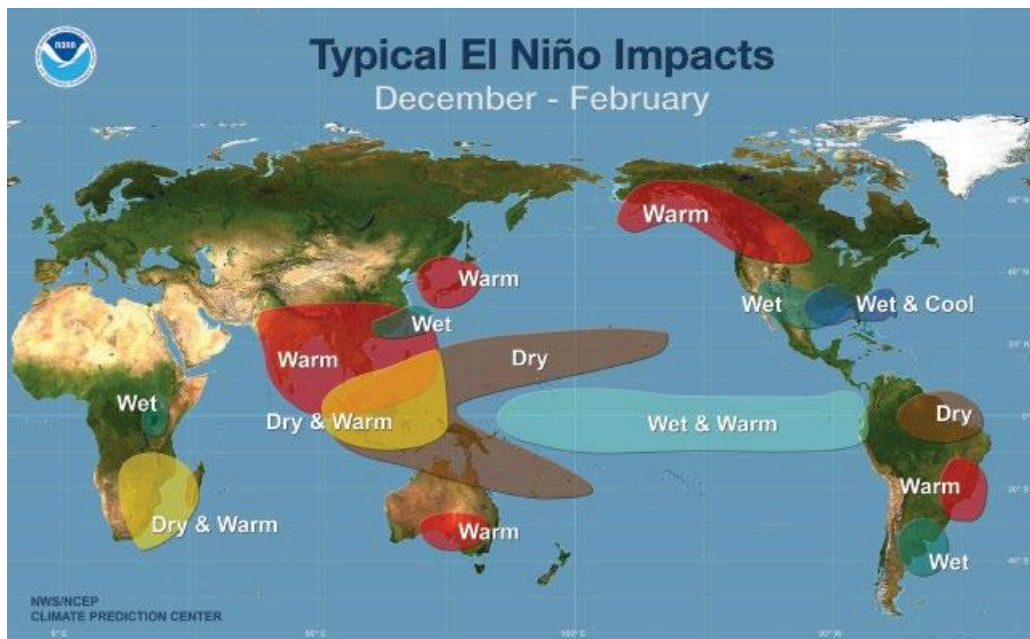


Figure 1.2: Typical impacts of El Niño (top) and La Niña (bottom) on global weather patterns during the peak season of development in December–February. Taken from NOAA/Climate Prediction Center.

Between 1997 and 1998, Ecuador experienced a large-scale El Niño event. During the development of this phenomenon, widespread flooding occurred in several areas of Ecuador caused by the heavy rains. In addition, it was recorded several landslides and destruction of crops caused by soil

erosion. All these events caused great damage to the country's infrastructure, causing the displacement of populations and even human losses²².

Conversely, La Niña events typically bring drier conditions to Ecuador, particularly affecting the coastal and inter-Andean regions. The strengthened trade winds during La Niña enhance the upwelling of cooler, nutrient-rich waters along the coast, leading to reduced sea surface temperatures and decreased rainfall¹⁸. La Niña events tend to bring cooler and wetter conditions to the highlands, which can benefit agriculture but also increase the risk of frost in higher elevations. This variability poses significant challenges for water resource management and agricultural planning in the Andean region, requiring adaptive strategies to mitigate the adverse impacts of ENSO cycles^{23 24}.

A notable La Niña event occurred in 1999-2000, bringing prolonged dry conditions that led to water shortages, affecting both agriculture and urban water supplies. Farmers in provinces such as Loja and Azuay faced severe drought, resulting in crop failures and economic losses. Additionally, the reduced rainfall impacted hydroelectric power generation, causing energy shortages in certain areas^{25 26}.



Figure 1.3: Floods in the city of Guayaquil (left) and La Camaronera (right) caused by the El Niño phenomenon, taken on February 19 and March 7 of 1998, respectively. Source: El Universo.

1.3 Predictability and Challenges

Recent advancements in satellite technology, oceanic and atmospheric monitoring systems, and climate models have significantly improved our understanding of ENSO mechanisms and their impacts. Enhanced climate models have increased our ability to predict ENSO events months in advance. Coupled ocean-atmosphere models have been particularly vital in understanding the feedback mechanisms

driving the dynamics of ENSO¹¹.

Furthermore, accurately predicting the onset, duration, and intensity of ENSO events remains a very difficult task. Despite continuous improvements in climate models, problems persist in capturing the timing and magnitude of ENSO events, especially when external factors such as volcanic activity or anthropogenic emissions are considered⁶. Another important problem is the variability of ENSO impacts, which makes it difficult to develop response strategies for affected regions. Indeed, the interactions between ENSO and other climate patterns, such as the Indian Ocean dipole, the Pacific decadal oscillation, and the Atlantic multidecadal oscillation, are not fully understood and may modulate or greatly amplify the effects of ENSO^{12,27}.

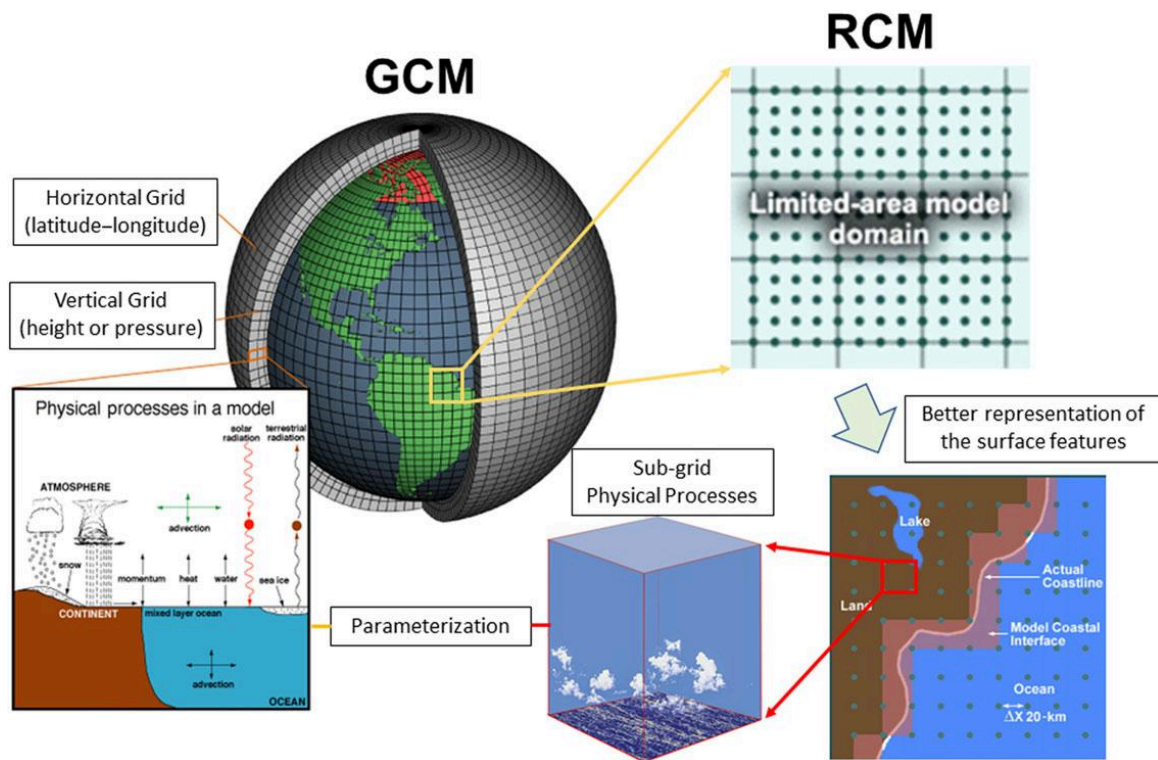


Figure 1.4: Illustration of a General Circulation Model (GCM) and a Regional Climate Model (RCM). GCMs simulate the climate system based on the fundamental laws of physics, chemistry, and biology, covering the entire globe. RCMs are specialized to simulate regional-scale climate processes more accurately by taking high-resolution factors into account, such as topography and coastlines. Taken from "The State of the Art and Fundamental Aspects of Regional Climate Modeling in South America"⁵

A recent concern is the possibility that some anthropogenic activities will alter and worsen the characteristics of ENSO. Indeed, recent research suggests that global warming may eventually alter the frequency, intensity, and spatial distribution of ENSO events, leading to extreme weather conditions²⁸. In this context, regional climate models (RCMs) are of paramount importance for understanding the

annual variability in climate caused by ENSO in a local domain like Ecuador. RCMs provide high spatial resolution, allowing for a detailed representation of local geographical features such as mountains, valleys, and coastlines, which is crucial for a country with diverse topography influencing its climate patterns. High-resolution models can capture the microclimates within the Andean highlands, coastal plains, and Amazon basin, often missed by global models²⁶.

The detailed outputs from RCMs assess the potential impacts of ENSO on local infrastructure, agriculture, and water resources, critical for developing adaptation strategies to mitigate adverse effects of ENSO-related extreme weather events²⁹. Finally, RCMs provide valuable information for policymakers and planners to develop targeted strategies for climate adaptation and disaster risk reduction, enabling more effective and tailored policies to address ENSO impacts at the regional level^{5 30}.

1.4 Research problem

Research has provided valuable insights into the climate dynamics of Ecuador and the impact of ENSO. Evaluations of high-resolution precipitation scenarios for the southern Ecuadorian Andes have contributed to understanding regional climate variability²⁶. This study emphasized the need for improved precipitation datasets and suggested further research to integrate local observational data to enhance model accuracy. Analyses of the forcings and evolution of the 2017 coastal El Niño provided detailed assessments of its impacts on northern Peru and Ecuador²⁰. Future research should focus on the combined effects of coastal and basin-wide El Niño events to better predict their impacts. Studies of present-day climate and projected future changes in temperature and precipitation in Ecuador have offered important projections under various climate scenarios³¹. This research stressed the importance of considering elevation-dependent warming and suggested further investigation into the potential feedback mechanisms between land use changes and climate. Furthermore, projected changes in climate, elevation-dependent warming, and extreme events over continental Ecuador for the period 2041-2070 have been examined, highlighting the need for detailed regional climate analyses³². This research pointed out the necessity for high-resolution climate models to capture microclimatic variations and suggested the inclusion of more extreme event scenarios in future studies.

Advances in regional climate modeling have greatly increased our understanding of climate variability and its impacts at the local level. RegCM in particular has shown very promising results in several areas. For example, in one study, by evaluating the modulation of large-scale signals produced by dynamically downscaled seasonal forecast systems, the use of RegCM demonstrated high accuracy in fitting global climate model outputs for regional applications³³. This study also recommends the

integration of different regional climate models to improve predictive capability in specific areas. Likewise, the study on rainfall in northeastern Brazil, by downscaling the Climate Forecast System Version 2 (CFSv2) model using RegCM-4.9, highlighted the importance of using regional climate models to capture global climate phenomena³⁴. In this study, the author suggests that future studies should focus on improving the representation of local atmospheric processes and land-ocean interactions to improve the prediction of precipitation patterns.

Despite these advancements, there remains a need to explore the effectiveness of different climate models in the Ecuadorian domain, particularly in the context of ENSO. This thesis aims to complement and build upon the existing body of research by utilizing the fifth-generation Regional Climate Modeling System (RegCM5). The novelty of this investigation lies in the application of RegCM5 to the Ecuadorian domain specifically to study the influence of ENSO, which has not been comprehensively explored in previous research. By leveraging advanced computational modeling, this study seeks to provide a more detailed characterization of temperature and precipitation variability associated with ENSO events. This improved modeling approach will enhance the understanding of ENSO-related climatic variations with high accuracy and a fine spatial resolution. It will allow for a more detailed assessment of the potential impacts of ENSO on the climate of Ecuador for the near future (2020-2040), providing valuable information for developing effective adaptation and mitigation strategies.

1.5 Objectives

1.5.1 General objective

This thesis aims to understand the impact of the El Niño Southern Oscillation (ENSO) on interannual climate variations in Ecuador, emphasizing the analysis of climatic parameters such as near-surface air temperature and precipitation through advanced computational modeling.

1.5.2 Specific objectives

The specific goals of this thesis are the following:

1. To model the climatic conditions of Ecuador under different ENSO phases (El Niño and La Niña) using the fifth-generation Regional Climate Modeling System (RegCM5).
2. To validate the performance of the RegCM5 model against ERA5 reanalysis data for the period 1991-2020, assessing its accuracy in simulating near-surface air temperature, total precipitation, wind divergence, and relative humidity across Ecuador, and to identify areas of model discrepancies.

3. To apply bias correction techniques, specifically Quantile Delta Mapping (QDM), to the RegCM5 model outputs to improve the accuracy of projections for near-surface air temperature and total precipitation, particularly during ENSO-related events.
4. To identify and analyze future ENSO events (2021-2050) using bias-corrected model data based on SST anomalies in the Niño 1+2 region, examining the frequency and characteristics of El Niño and La Niña events.
5. To investigate the potential impacts of ENSO on the climate of Ecuador for the near-future (2021-2050), focusing on changes in temperature and precipitation patterns during El Niño and La Niña events, and to provide detailed projections of spatial distribution and intensity of these climatic variables.

Chapter 2

Methodology

This study aims to understand the impact of the El Niño-Southern Oscillation (ENSO) on interannual climate variations in Ecuador. By employing the Regional Climate Modeling System RegCM5 (version 5.0.0), we perform long-term simulations to analyze the influence of ENSO on climatic parameters and predict potential future changes. The use of high-resolution regional climate models is crucial for capturing the complex interactions between the atmosphere and ocean, especially in a region with diverse topography like Ecuador⁵.

2.1 Software

The Regional Climate Modeling System (RegCM5) is an advanced climate simulation tool developed by the Abdus Salam International Centre for Theoretical Physics (ICTP) *. For this study, we used the most recent version, RegCM5 (version 5.0.0), which has shown improvements in computational efficiency and accuracy compared to previous versions. This model incorporates a new non-hydrostatic dynamical core called MOLOCH, which according to tests performed optimizes the representation of complex atmospheric processes and topographic effects³⁵, which makes it a very useful tool for studies in regions with complex geography, such as Ecuador.

2.1.1 RegCM5 Preprocessor

Domain

The domain for simulation, illustrated in Figure 2.1, is centered at 4°S, 82.5°W, covering all of continental Ecuador and extending into the Pacific Ocean to include the Niño 1+2 region, essential for studying ENSO-related phenomena. The simulation grid, with a resolution of 25 km, consists of 93

*The RegCM5 model is available at <https://github.com/ICTP/RegCM>, and more details about ICTP can be found at <https://www.ictp.it/>.

cells along the x-axis and 89 cells along the y-axis, vertically extending across 23 levels up to 5hPa. This high resolution enables a detailed representation of local geographical features, such as the Andes mountains, the Pacific coastal plains, and the Amazon basin, which significantly influence regional climate patterns in Ecuador³¹.

The topography of Ecuador is diverse and complex. The Andes mountain range runs from north to south, with peaks exceeding 6,000 meters, creating varied climatic zones. The coastal region at sea level experiences different climate conditions compared to the high-altitude areas³⁶. The Galapagos Islands, located about 1,000 km off the coast, also present unique topographical features that affect the local climate. Including the El Niño region 1+2 in the simulation domain is critical because it is one of the primary areas where the SST anomalies are most pronounced during ENSO events, significantly impacting regional weather patterns¹⁸.

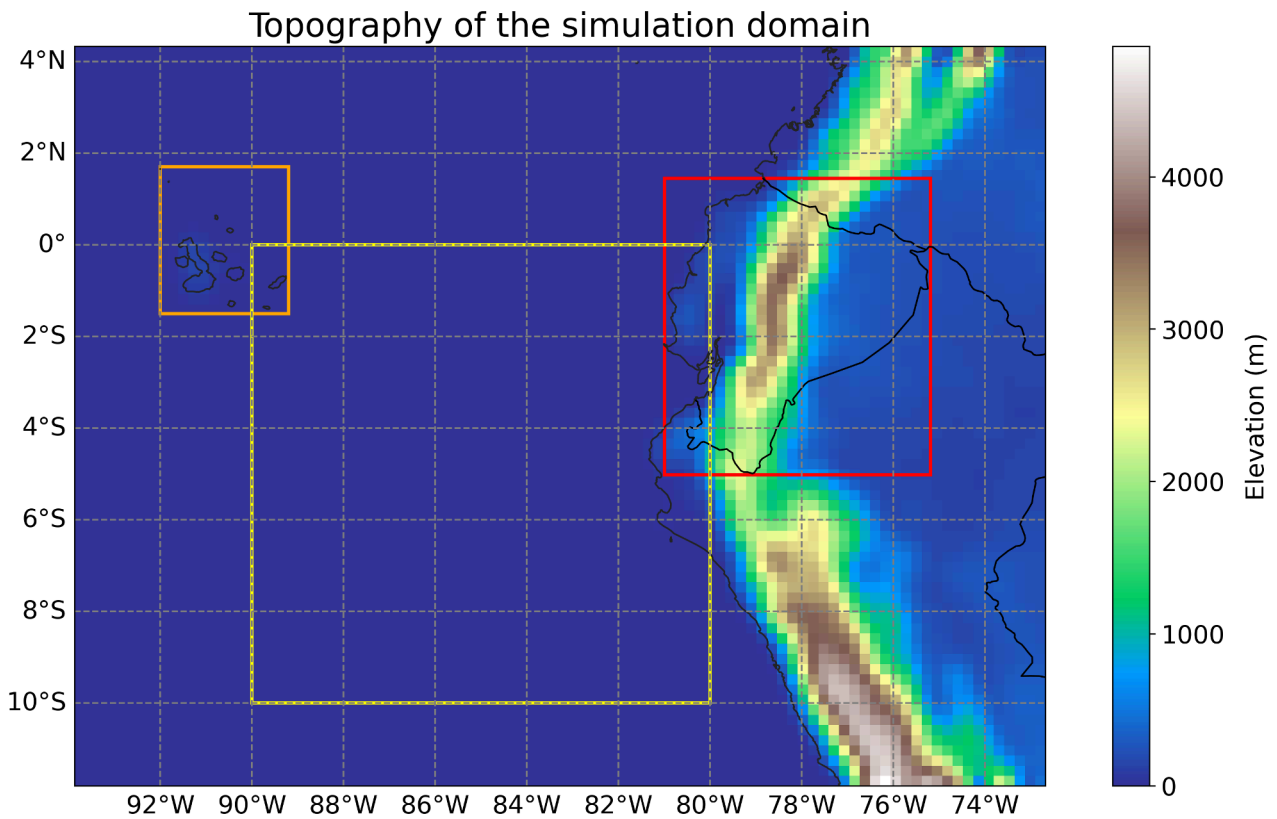


Figure 2.1: Topography of the simulation domain for both the present and near-future period. The red square encloses the continental region of Ecuador. The orange square encloses the Galapagos Islands, and the yellow square encloses the El Niño 1+2 region. These three squares conform to our target area of study.

Initial and Boundary Conditions

RegCM5 realizes the downscaling process by employing one-way nesting techniques to derive boundary conditions from General Circulation Models (GCMs). This method allows regional climate simulations to be informed by larger-scale climate dynamics without feedback to the GCM, ensuring that the regional model benefits from the boundary conditions imposed by the global model while maintaining computational efficiency³⁵.

For this study, the initial and boundary conditions are provided by the HadGEM2-ES GCM. HadGEM2-ES is a coupled Atmosphere-Ocean General Circulation Model (AOGCM) documented in detail in Collins et al. 2011³⁷. The atmospheric component of HadGEM2-ES has a horizontal resolution of N96 ($1.875^\circ \times 1.25^\circ$) with 38 vertical levels, while the ocean component has a horizontal resolution of 1° (increasing to $1/3^\circ$ at the equator) and 40 vertical levels³⁸. A previous study³⁹ showed that HadGEM2-ES provided reliable boundary conditions that helped improve the accuracy of regional climate simulations in representing ENSO-related climate variability in South America.

Data for the simulations were obtained from the RegCM repository, utilizing variables such as specific humidity (hus), air temperature (ta), zonal wind (ua), meridional wind (va), and surface pressure (ps). The simulations follow the RCP8.5 scenario, which represents a high greenhouse gas concentration pathway. The RCP8.5 scenario was chosen for this study because it represents a high greenhouse gas concentration pathway, often referred to as the "business-as-usual" scenario. This scenario assumes continued increases in greenhouse gas emissions throughout the 21st century, resulting in significant radiative forcing of 8.5 W/m^2 by 2100⁴⁰. The selection of RCP8.5 allows for the examination of potential climate impacts under extreme conditions, providing valuable insights into the worst-case outcomes of climate change. By using this scenario, the study aims to understand the upper bounds of climate variability and change, which is crucial information for developing robust adaptation and mitigation strategies to address the severe consequences of high-emission trajectories in Ecuador.

2.1.2 RegCM5 Simulation

Mesh Details

The horizontal grid in RegCM5 uses the Arakawa C grid system, a staggered grid arrangement where velocity components and scalar quantities (like temperature and humidity) are computed at different points within each grid cell. This design enhances the accuracy and stability of numerical simulations by reducing computational errors associated with interpolating between different types of variables. The C grid system is particularly effective for representing atmospheric dynamics and resolving fine-

scale features in the model domain⁴¹.

Vertically, RegCM5 uses a height-based coordinate system, which is effective for capturing the complex vertical structure of the atmosphere, especially in areas with significant topographical variations like Ecuador. This vertical coordinate system follows the terrain, allowing a more precise depiction of surface influences on atmospheric processes³⁹.

For our model, we use the Mercator map projection, as it preserves angles and provides a fairly accurate representation of geographic features near the equator. This feature is quite useful for our domain and guarantees minimal distortion of spatial characteristics. Regarding the boundary conditions, it is important to ensure a smooth transition between the regional model and the GCM inputs. Therefore, we used 12 grid cells at each domain boundary as a transition zone, in which the GCM was applied. the exponential relaxation method. This method gradually adjusts the regional model solution to the boundary conditions provided by the GCM, providing stability to the model near the domain boundaries.³⁵.

Model Equations

For these simulations, we used the MOLOCH dynamical core, implemented in RegCM5, which solves a set of fully compressible, non-hydrostatic equations. This model uses a hybrid terrain-following vertical coordinate, ζ , that adapts to the topography and extends from the surface to a configurable model top (rigid lid) where the vertical velocity is set to zero³⁵. The MOLOCH dynamical core is particularly suited for high-resolution simulations where atmospheric processes like convection and wave propagation are explicitly resolved without hydrostatic balance assumptions.⁴².

The hybrid ζ coordinate is defined over the interval $[0, Z_{\text{top}}]$, with Z_{top} representing the configurable top of the model. The relationship between the model height and the ζ coordinate is given by the following equation:

$$z = h(x, y)G(\zeta) + Z_f e^{\frac{\zeta}{H}-1} \quad (2.1)$$

where $h(x, y)$ represents the model topography, Z_f is a scaling factor, H is the atmospheric scale height, and $G(\zeta)$ is a polynomial function of ζ that defines the stretching of vertical levels. This function allows for higher resolution near the surface and coarser resolution at higher altitudes³⁵.

The horizontal and vertical discretization uses the Arakawa-C grid, where wind components are staggered relative to other variables. So, the generalized vertical velocity is given by the following

expression:

$$\frac{\partial \zeta}{\partial t} = s = F_z \left[w - \left(u \frac{\partial h}{\partial x} + v \frac{\partial h}{\partial y} \right) G \right] \quad (2.2)$$

where F_z is a time-independent function that depends on the ζ coordinate, u and v are the eastward and northward components of velocity, respectively, and h is the topography. This formulation allows the model to account for terrain-following effects while ensuring an accurate representation of vertical motion.

The model solves the governing equations using the Exner function, Π , and the virtual potential temperature, Θ_v , as the primary prognostic variables. These variables are related to temperature, pressure, and moisture content:

$$\Pi = \left(\frac{P}{P_0} \right)^{\frac{R_d}{c_{pd}}} \quad (2.3)$$

$$\Theta_v = \frac{T_v}{\Pi} \quad (2.4)$$

$$T_v \approx T (1 + 0.61q_v - q_c - q_i) \quad (2.5)$$

where P is the pressure, P_0 is a reference pressure, R_d is the gas constant for dry air, c_{pd} is the specific heat of dry air at constant pressure, T_v is the virtual temperature, and q_v , q_c , q_i are the mass mixing ratio of water vapor, liquid water and ice water. The use of Π and Θ_v provides a more efficient formulation for moist atmospheric dynamics, capturing the effects of temperature and humidity in a single equation³⁵.

Now, the momentum equations for the horizontal wind components, u and v , and the vertical velocity, w , are expressed as:

$$\frac{du}{dt} = mc_{pd}\Theta_v \frac{\partial \Pi}{\partial x} - mG(\zeta) \frac{\partial h}{\partial x} \left(g + \frac{dw}{dt} \right) + f_v + K_u \quad (2.6)$$

$$\frac{dv}{dt} = mc_{pd}\Theta_v \frac{\partial \Pi}{\partial y} - mG(\zeta) \frac{\partial h}{\partial y} \left(g + \frac{dw}{dt} \right) - f_u + K_v \quad (2.7)$$

$$\frac{dw}{dt} = -F_z c_{pd} \Theta_v \frac{\partial \Pi}{\partial z} - g + K_w \quad (2.8)$$

where g is the gravitational acceleration, The terms K_x denote the physical parameterizations, and f_u , f_v the Coriolis terms, which are essential for capturing the effects of Earth's rotation on atmospheric flows, especially at larger scales, such as synoptic and planetary scales⁴³.

Additionally, The thermodynamic equation describes the temporal evolution of the virtual potential

temperature, Θ_v , including the effects of advection and diabatic heating:

$$\frac{d\Theta_v}{dt} \approx K_{\Theta_v} \quad (2.9)$$

where K_{Θ_v} represents the contributions from diabatic processes, such as latent heat release during condensation and radiative heating or cooling³⁵.

On the other hand, the continuity equation is solved in flux form to ensure mass conservation, expressed as:

$$\frac{d\Pi}{dt} \approx -\Pi \frac{R_d}{C_{vd}} m^2 \left\{ F_z \left[\frac{\partial \left(\frac{u}{mF_z} \right)}{\partial x} + \frac{\partial \left(\frac{v}{mF_z} \right)}{\partial y} \right] + \frac{\partial \left(\frac{s}{F_z} \right)}{\partial \zeta} \right\} \quad (2.10)$$

where $c_{v,d}$ is the specific heat for dry air at constant volume. In this formulation, explicit diffusion is unnecessary for maintaining numerical stability. Instead, stability is achieved by applying a second-order spatial filter to the divergence of the horizontal wind, effectively smoothing out small-scale numerical noise without compromising the physical accuracy of the model³⁵.

RegCM5 uses a variety of numerical methods to solve these equations efficiently. The model uses a second-order centered finite difference scheme for the spatial derivatives, which provides a perfect balance between accuracy and computational cost. This method calculates the derivatives by averaging the values at adjacent grid points, which helps to reduce numerical errors. To advance the solution in time, the model uses an explicit temporal integration scheme. The model applies an explicit splitting method, where fast-moving gravity waves are handled with a smaller time step to ensure stability, while slower processes are integrated with a larger time step. Furthermore, as already mentioned the model employs a hybrid vertical coordinate that follows the terrain, combining the advantages of pressure and height coordinates. This coordinate system improves the ability of the model to accurately simulate complex terrain and severe weather phenomena³⁵.

Physical parameterizations

RegCM5 employs physical parameterizations to simulate atmospheric processes occurring at scales too small for our grid resolution to capture. These parameterizations are crucial to represent the complex interactions between the atmosphere, land surface, and ocean³⁵. The parameterization schemes we use in this study are:

- Radiation: modified NCAR CCM3 scheme RegCM5 uses a radiation parameterization adapted from the NCAR CCM3 radiative transfer scheme⁴⁴. This scheme is responsible for calculating the motion of solar and terrestrial radiation through the atmosphere, taking into account the effect of gases such as CO_2 , O_3 , and water vapor, as well as that of clouds and aerosols. In

this scheme, the shortwave component uses the δ -Eddington approximation, which takes into account scattering and absorption by atmospheric particles. Likewise, the longwave component includes the effects of gaseous absorption and emission, here the radiative properties of the clouds are parameterized as a function of liquid water content and droplet size.

- Planetary Boundary Layer (PBL): Modified Holtslag Scheme The modified Holtslag scheme⁴⁵ is used to represent turbulence and vertical mixing in the planetary boundary layer (PBL). This non-local diffusion scheme accounts for the counter-gradient fluxes resulting from large-scale eddies in an unstable, well-mixed atmosphere. The eddy diffusivity (K_c) is given by:

$$K_c = kw_tz\left(1 - \frac{z}{h}\right)^2 \quad (2.11)$$

where k is the von Karman constant, w_t is the turbulent convective velocity, z is the height, and h is the PBL height. The counter-gradient term γ_c for temperature and water vapor is:

$$\gamma_c = C \frac{\phi_c^0 w_t h}{\theta_s} \quad (2.12)$$

where C is a constant, ϕ_c^0 is the surface flux of the variable, and θ_s is the surface potential temperature. This scheme effectively captures the vertical transport of heat, moisture, and momentum, which are essential for accurate weather and climate simulations.

- Cumulus Convection: Mixed Scheme (Grell and MIT Emanuel) For cumulus convection, a mixed scheme is employed, combining the Grell scheme⁴⁶ over land and the Emanuel and Zivkovic-Rothman scheme⁴⁷ over the ocean. This approach was suggested by Reboita et al. 2014⁴⁸, who found that this was the best configuration for simulating both precipitation and air temperature for the subdomain AN1 which includes the border between Ecuador and Perú. The Grell scheme considers clouds as two steady-state circulations (updraft and downdraft) with no direct mixing between the cloudy air and environmental air[†], except at the top and bottom of the circulations. The mass flux approach used in the Grell scheme allows for detailed simulation of convective processes based on environmental conditions. The MIT Emanuel scheme assumes highly episodic and inhomogeneous mixing in clouds. Convection is triggered when the level of neutral buoyancy is greater than the cloud base level. The cloud model includes sub-cloud-scale updrafts and downdrafts, with entrainment and detrainment rates depending on the vertical gradients of buoyancy. This detailed representation of convective processes improves the simulation of precipitation and temperature over the ocean.

[†]In this context, "cloudy air" refers to the air mass within the cloud, characterized by higher moisture content and cloud particles, whereas "environmental air" refers to the surrounding air mass outside the cloud.

- Land Surface Model: CLM4.5 The Community Land Surface Model version 4.5 (CLM4.5)⁴⁹ serves to represent the land surface processes (soil moisture, evapotranspiration, vegetation types, and the carbon cycle). This scheme tries to capture all these processes within each climate model cell with a "mosaic" approach. The hydrological and energy balance equations are solved in the cells according to the land cover type. These equations are solved at the same time as the main hydrological steps, to ensure the representation of the interaction between the processes at the Earth's surface and the atmospheric model. This scheme was selected because it has proven to be very accurate in simulating energy, water, and carbon exchanges between the Earth's surface and the atmospheric atmosphere.
- Microphysics: SUBEX Scheme The SUBEX (Subgrid Explicit Moisture Scheme)⁵⁰ handles cloud and precipitation processes, accounting for sub-grid variability in clouds. The cloud fraction (FC) is determined by the relative humidity (RH):

$$FC = \sqrt{\frac{RH - RH_{\min}}{RH_{\max} - RH_{\min}}} \quad (2.13)$$

Precipitation (P) forms when cloud water content exceeds a threshold (Q_{th}):

$$P = C_{\text{ppt}} \left(\frac{Q_c}{FC} - Q_{th} \right) FC \quad (2.14)$$

where C_{ppt} is the conversion rate, Q_c is the cloud water content, and Q_{th} is the autoconversion threshold. This scheme also includes formulations for raindrop accretion and evaporation, which are essential for understanding cloud dynamics, precipitation formation, and their impact on climate.

- Ocean Fluxes: Zeng Scheme The Zeng scheme⁵¹ models the exchanges of momentum, heat, and moisture between the ocean surface and the atmosphere. It accounts for stability conditions and includes a gustiness velocity \ddagger to represent the additional flux induced by boundary layer scale variability. The fluxes are calculated using bulk aerodynamic formulas:

$$\tau = \rho_a u_*^2 (u_x^2 + u_y^2)^{1/2} / u \quad (2.15)$$

$$SH = -\rho_a C_{pa} u_* \theta_* \quad (2.16)$$

[‡]"Gustiness" refers to the variability and fluctuations in wind speed due to turbulence and other small-scale processes in the atmospheric boundary layer.

$$LH = -\rho_a L_e u_* q_* \quad (2.17)$$

where τ is the momentum flux, SH is the sensible heat flux, LH is the latent heat flux, u_* is the friction velocity, θ_* is the temperature scaling parameter, q_* is the specific humidity scaling parameter, ρ_a is air density, C_{pa} is the specific heat of air, and L_e is the latent heat of vaporization. This scheme is crucial for accurately modeling sea surface temperatures and their influence on atmospheric conditions.

2.2 Hardware

The computational requirements for running high-resolution climate models such as the Regional Climate Modeling System (RegCM5) are substantial, and utilizing a high-performance computing (HPC) cluster is essential for handling these demands efficiently.

In this study, simulations were performed on two high-performance computing (HPC) clusters: one provided by the Ecuadorian Corporation for the Development of Research and Academia (CEDIA) and one external. The system consisted of 24 compute nodes, each with 31 Intel Xeon Platinum 8174 processors, for a total of 744 processors. In addition, each node had 128 GB of RAM and we used approximately 3 TB of storage space, including the GCM data and simulation results. For data transfer between the HPC centers, SSH protocols were used.

2.3 Data Analysis

The data analysis component of this research is designed to validate the Regional Climate Modeling System (RegCM5) outputs against observational datasets and investigate future projections of climatic variables in Ecuador under different phases of the El Niño-Southern Oscillation (ENSO).

2.3.1 Preprocessing Data

To validate the simulated data of our model for the present time (1991 - 2020), we use the "ERA5 monthly averaged data on single levels from 1940 to present" dataset downloaded from the Copernicus Climate Data Store ^{§52}. The original $0.25^\circ \times 0.25^\circ$ grid was remapped onto a 25km x 25km grid to ensure compatibility with our model output. On the other hand, the model data for the present

[§]The Copernicus Climate Data Store provides access to climate data from ECMWF: <https://cds.climate.copernicus.eu/cdsapp#!/home>. The specific ERA5 dataset is available at: <https://cds.climate.copernicus.eu/cdsapp#!/dataset/reanalysis-era5-single-levels-monthly-means?tab=overview>.

and near-future time, initially recorded at 6-hour intervals, were aggregated into monthly averages. Subsequently, the boundary relaxation areas from the model data were trimmed to eliminate potential inaccuracies due to edge effects and numerical artifacts commonly associated with boundary regions in climate models. This preprocessing step resulted in comparable datasets for each variable, covering the same spatial area with identical resolution and frequency.

2.3.2 Model Validation

The model simulation for the current period spanned from 1991 to 2020. To assess the accuracy of our model, we first calculated annual averages of several climate variables and compared them to annual averages obtained from the ERA5 dataset. We calculated the annual mean by averaging the monthly values of each variable for each year. This method provides information about the overall trends and long-term behavior of the variables, effectively smoothing out short-term fluctuations⁵³. The variables we analyzed in this study were:

- **Near-Surface Air Temperature**, which represents the air temperature at 2 meters above the ground level⁵⁴.
- **Total precipitation**, which encompasses all forms of water, including rain, snow, sleet, and hail, that falls to the ground over a specified period⁵⁵.
- **Wind divergence** at specific altitudes (10 and 100 meters), which indicates the rate at which air spreads out horizontally. Positive divergence implies air is spreading out, while negative divergence indicates air is converging⁴³. The divergence of the wind field $\mathbf{V}(u, v)$, where u is the wind component in the x direction (Eastward winds) and v is the wind component on the y direction (Northward winds), was calculated using the MetPy package³ and with the formula:

$$\nabla \mathbf{V}(u, v) = \frac{\partial u}{\partial x} + \frac{\partial v}{\partial y}$$

- **Specific humidity** is the mass of water vapor per unit mass of moist air. It is a measure of the actual amount of moisture in the air⁵⁶.
- **Relative humidity** is the ratio of the current amount of water vapor in the air to the maximum amount of water vapor the air can hold at a given temperature⁵⁷.

Since, unlike our model, the ERA5 dataset does not include relative and specific humidity within its climate variables, it was necessary to perform calculations based on others. Particularly for specific humidity, we used the formula:

$$q = 0.622 \cdot \left(\frac{e_d}{P - 0.378 \cdot e_d} \right)$$

where q is the specific humidity, T is the near surface air temperature, e_d is the dew point vapor pressure, P is the surface pressure and e_s is the saturation vapor pressure given by:

$$e_s = 6.112 \cdot \exp\left(\frac{17.67 \cdot T}{T + 243.5}\right)$$

And, the formula for the relative humidity was given by:

$$RH = 100 \cdot \left(\frac{e_d}{e_s} \right)$$

The comparison was carried out by generating maps of these climate variables from both the model output and the ERA5 dataset, as well as the bias between them. Subsequently, several error metrics were calculated:

- **MAE (Mean Absolute Error):** This metric measures the average magnitude of errors between observed and predicted values, providing a straightforward indication of model accuracy⁵⁸.

$$MAE = \frac{1}{n} \sum_{i=1}^n |P_i - O_i|$$

- **RMSE (Root Mean Squared Error):** This metric computes the square root of the average squared differences between observed and predicted values, penalizing larger errors more heavily⁵⁹.

$$RMSE = \sqrt{\frac{1}{n} \sum_{i=1}^n (P_i - O_i)^2}$$

- **Median Bias:** This metric is a statistical measure that indicates the central tendency of differences between predicted and observed values. Unlike mean bias, median bias is less sensitive to outliers and provides a robust assessment of the systematic error of the model⁶⁰.

$$\text{Median Bias} = \text{Median}(P_i - O_i)$$

- **Pearson Correlation:** This metric assesses the linear relationship between observed and predicted values, providing insights into the ability of the model to replicate variability⁶¹.

$$r = \frac{\sum_{i=1}^n (O_i - \bar{O})(P_i - \bar{P})}{\sqrt{\sum_{i=1}^n (O_i - \bar{O})^2} \sqrt{\sum_{i=1}^n (P_i - \bar{P})^2}}$$

- **Willmott Index:** This metric measures the degree of agreement between observed and predicted values, considering both the magnitude and direction of errors⁶².

$$d = 1 - \frac{\sum_{i=1}^n (P_i - O_i)^2}{\sum_{i=1}^n \left(|P_i - \bar{O}| + |O_i - \bar{O}| \right)^2}$$

where P_i represents the predicted values, O_i represents the observed values, n is the number of observations, and \bar{O} and \bar{P} are the means of the observed and predicted values, respectively.

In addition, to analyze the representation by the model of ENSO phenomena, composite maps were computed for the El Niño and La Niña events. The Oceanic Niño Index (ONI), which is the three-month running mean of sea surface temperature anomalies in the Niño 3.4 region, was used to determine the months for each type of event⁸. Then, monthly averages for El Niño and La Niña events were computed and compared with those from the ERA5 data.

2.3.3 Bias Correction

In order to reduce any systematic biases identified during the validation process, we apply bias correction to the model outputs. This statistical technique adjusts climate model outputs to more closely align with observed data. This adjustment is essential because although climate models are powerful tools for forecasting future climate conditions, they often exhibit systematic errors or biases. Correcting these biases using observed climatological data or reanalysis data greatly improves the reliability and accuracy of climate model projections⁶³.

The method we selected for bias correction in this study is quantile delta mapping (QDM). QDM is an advanced bias correction technique that modifies the quantiles of model outputs based on the observed data, ensuring that both the distribution and trends of the data are maintained. This technique is especially effective in handling non-stationary biases, which are biases that change over time⁶⁴. The process begins with quantile mapping, which adjusts the cumulative distribution function (CDF) of the model outputs to align with the CDF of the observed data. For a specific quantile q , the quantile mapping adjustment is:

$$x_q^{\text{QM}} = F_{\text{obs}}^{-1}(F_{\text{mod}}(x_q))$$

where x_q^{QM} is the quantile-mapped value at quantile q , F_{obs} is the CDF of the observed data, F_{mod} is the CDF of the model data, and x_q is the model data at quantile q . Subsequently, the delta change adjustment is applied to preserve the trends in the model data. The quantile delta change is calculated from the historical period and then applied to the future period. The delta change for a specific quantile q is:

$$\Delta x_q = F_{\text{mod,fut}}^{-1}(F_{\text{mod,hist}}(x_q^{\text{hist}})) - x_q^{\text{hist}}$$

where Δx_q is the delta change at quantile q , $F_{\text{mod,fut}}$ is the CDF of the future model data, $F_{\text{mod,hist}}$ is the CDF of the historical model data, x_q^{hist} is the historical model data at quantile q . Finally, the delta change is applied to the quantile-mapped values to obtain the bias-corrected future projections. The bias-corrected value x_q^{QDM} at quantile q is:

$$x_q^{\text{QDM}} = x_q^{\text{QM}} + \Delta x_q$$

This ensures that the corrected model data not only matches the observed distribution but also accurately reflects the projected changes. Nonetheless, before applying this bias correction method to our near-future simulation data, we first need to validate it.

To validate the bias correction, both the present simulated data and the ERA5 data were split into two parts: one for calibration (1991-2010) and the other for validation (2011-2020). The `cmeth` package was then used to correct the validation data, the QDM technique from this package allows for an Additive QDM (compute absolute changes in quantiles) or a Multiplicative QDM (compute relative changes in quantiles)⁶⁵. After applying the bias correction to the validation part of the data, annual means of near-surface air temperature and total precipitation were calculated and compared. These variables are the most affected by El Niño and La Niña events. As with the model validation, maps of the corrected model, ERA5 data, and the bias between the two were plotted, and all error metrics were calculated.

In addition, we also calculated the annual cycles for these variables (using both the original and corrected data) and compared them to those obtained from the ERA5 data. This annual cycle helps us observe the typical behavior of these variables over a year, which we calculate by averaging the monthly values of each variable over the 30 available years. The comparison between these three cycles will help us assess whether the bias correction method also adjusts for the seasonal patterns of the variables.

2.3.4 Identification of El Niño and La Niña Events

For the analysis of future ENSO impacts, it is crucial to consistently identify ENSO events across different datasets. The domain of our simulation covers the Niño 1+2 region, which is one of the key areas for monitoring the ENSO phenomenon. The Niño 1+2 region is located in the eastern equatorial Pacific, specifically between 0-10°S and 90°W-80°W. This region is relevant because SST anomalies here are indicative of the onset and intensity of El Niño and La Niña events⁸.

For our study, it is also important to verify the effect that bias correction has on the El Niño 1+2 region, because this region is key for the subsequent identification of ENSO events. Therefore, we calculated the 3-month moving average of sea surface temperatures in this region. We did this with our corrected data and with the ERA5 data for comparison. This 3-month moving average is a smoothing technique that averages SSTs over three consecutive months, which reduces short-term fluctuations and highlights long-term trends. This allows us to better capture ENSO signals. Then, we proceeded to evaluate the similarity between both data sets, this comparison is important since the consistent SST patterns between our model and the ERA5 data are the basis for the identification of ENSO events.

It has to be noted that RegCM5 only models the atmosphere and is not coupled with an ocean model. By default in RegCM, SST is prescribed every six hours from temporally interpolated weekly or monthly SST products. These products, produced from satellite retrievals and in-situ measurements, represent the mean temperature in the top few meters of the ocean. Additionally, a prognostic SST scheme based on a two-layer model is implemented to improve the calculation of diurnal fluxes over the ocean³⁵. This is why comparing peaks in this region is crucial, as consistent SST patterns between the model and observations are essential for accurately identifying ENSO events.

We then calculate SST anomalies in the Niño 1+2 region to identify El Niño and La Niña events. Anomalies represent SST deviations from the long-term mean and are critical for classifying ENSO events. For this classification, we use the same thresholds as the Coastal El Niño Index (CEE), which provides specific criteria for identifying El Niño and La Niña events based on SST anomalies⁶⁶. According to this index, El Niño events are identified by SST anomalies greater than 0.4 °C for three consecutive months, while La Niña events are determined by SST anomalies less than -0.4 °C for the same period⁶⁷.

These thresholds were selected because they provided the greatest concordance between the El Niño and La Niña events in our model and those reported by the Oceanic Niño Index (ONI). Although we did not use the exact reference climatology specified by the ICEN, we adapted these thresholds to the climatology of our 30-year simulation period. This adaptation is necessary because we will use

these thresholds to determine El Niño and La Niña events for our near-future simulation.

2.3.5 Near-Future Projections

To analyze future climate conditions, the annual means of near-surface air temperature and precipitation for the near-future period (2021-2050) were computed and compared to the present simulation results. This comparison highlights the expected shifts in climate patterns and provides insights into long-term trends.

For this period, El Niño and La Niña years were identified using SST anomalies in the Niño 1+2 region. The same thresholds from the Coastal El Niño Index (ICEN) were applied to ensure consistency in identifying ENSO events. Using the identified ENSO events for the near-future simulation period, composite maps for El Niño and La Niña events were created. These composites represent the mean values of the selected climate variables during the ENSO events and offer a detailed understanding of the expected climatic impacts of ENSO under future conditions.

Chapter 3

Results

This chapter presents the results of the RegCM5 simulations for the present period (1991-2020) and near-future projections (2021-2050). The analysis includes the validation of near-surface air temperature, total precipitation, wind divergence at 10m and 100m, specific humidity, and relative humidity against ERA5 reanalysis data. Furthermore, the chapter details the application of bias correction techniques to improve the accuracy of the model simulations. The identification of El Niño and La Niña events and their impacts on climatic variables is also discussed. Finally, the near-future projections for near-surface air temperature and precipitation are analyzed to understand potential climate changes in Ecuador.

3.1 Validation of the Present Simulation (1991-2020)

3.1.1 Near-Surface Air Temperature

The climate of Ecuador is highly diverse, varying significantly across regions due to its geographical location on the equator and its varying topography, including coastal areas, the Andes highlands, and the Amazon rainforest⁶⁸. Near-surface air temperature is a key variable analyzed, as it influences and reflects the overall climate conditions in these regions. The annual mean surface air temperature in Ecuador typically ranges from 20°C to 25°C in the coastal and Amazon regions, with cooler temperatures in the highlands, averaging around 10°C to 20°C. The coastal regions experience relatively stable temperatures year-round due to the moderating influence of the Pacific Ocean, while the highlands exhibit more significant temperature variations due to altitude⁶⁸.

Figure 3.1 shows that the RegCM5 simulation captures this general pattern of air surface temperatures over Ecuador. However, there are noticeable differences, particularly along the Pacific coast and the highlands, where the model tends to overestimate temperatures, which is indicated by the red areas on the bias maps. The metrics registered in Table 3.1 suggest that the model performs well in

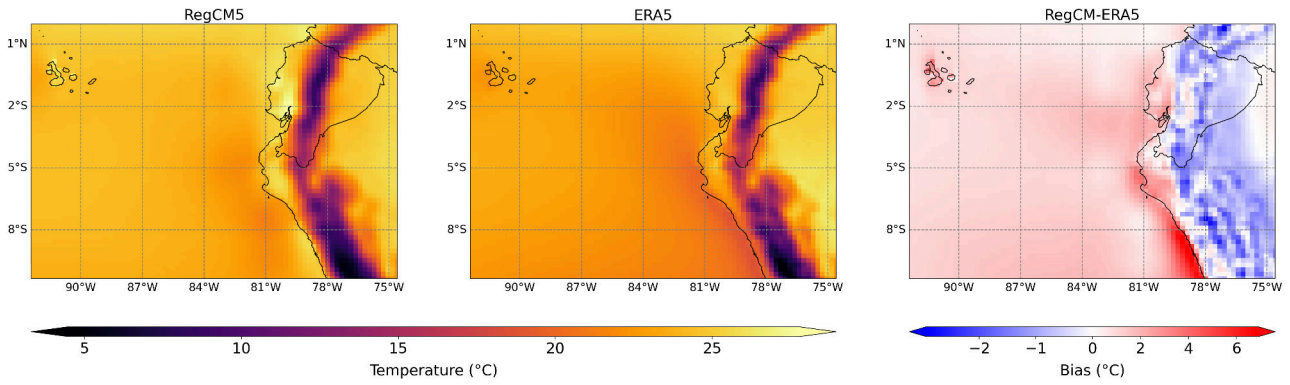


Figure 3.1: Annual mean near-surface air temperature from RegCM5 simulation (left), ERA5 reanalysis data (middle), and the bias between them (right) for the period 1991-2020. The bias map highlights areas where the RegCM5 simulation overestimates temperatures, particularly along the Pacific coast, the Andes highlands, and the Insular region (shown in red), and areas where it underestimates temperatures, such as parts of the Amazon basin and some regions within the Andes (shown in blue).

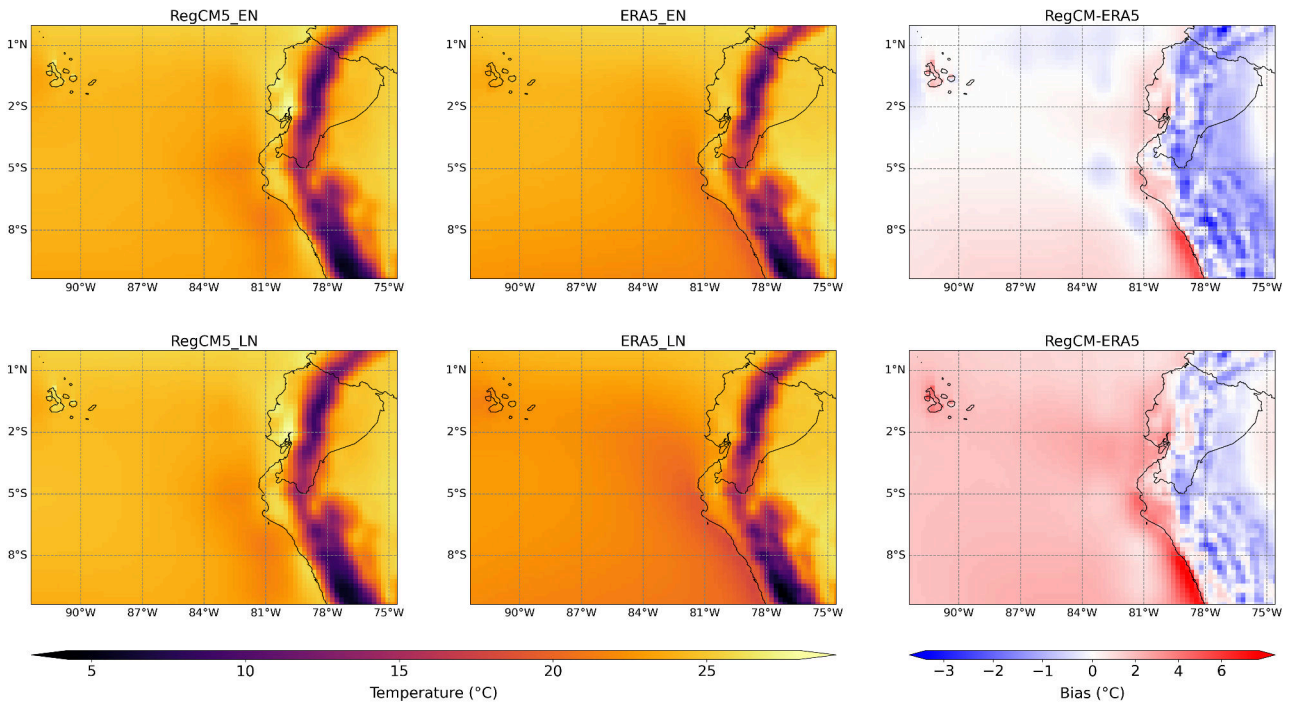


Figure 3.2: Composite near-surface air temperature for El Niño (top row) and La Niña (bottom row) events from RegCM5 simulation (left), ERA5 reanalysis data (middle), and the bias between them (right) for the period 1991-2020. During El Niño events, RegCM5 simulation overestimates temperatures along the Pacific coast and in the insular region (shown in red), while underestimating temperatures within the Andean and Amazon regions (shown in blue). During La Niña events, the model overestimates temperatures in the highlands of the Andes, as well as in some areas of the coastal and insular regions (shown in red), while underestimating temperatures within the Andes and Amazon areas (shown in blue).

Table 3.1: Error Metrics for Near-Surface Air Temperature

Metric	Annual Mean	El Niño Event	La Niña Event
MAE (°C)	1.12	0.64	1.60
RMSE (°C)	1.34	0.92	1.86
Bias (°C)	0.95	0.09	1.76
Correlation	0.95	0.97	0.93
Willmott Index	0.96	0.98	0.93

capturing the spatial variability of near-surface air temperature, indicated by the high Willmott Index and Pearson Correlation, but has systematic biases represented by the low MAE and RMSE. The median bias of 0.95°C suggests that the model tends to predict warmer conditions than those recorded.

During El Niño events, Ecuador generally experiences higher-than-average temperatures, particularly in the coastal and Amazon regions. This warming is due to the influx of warmer ocean currents from the central and eastern Pacific, which increases the SST and consequently, the air temperature⁶⁶. In Figure 3.2 we can observe how The RegCM5 simulation closely aligns with the ERA5 data during El Niño events, particularly in the coastal regions where the warming effect is most pronounced. The metrics registered in Table 3.1 indicate very low errors, which suggests that the model effectively captures the temperature anomalies associated with El Niño. In addition, the higher Willmott Index and Pearson Correlation during El Niño events highlight the ability of the model to replicate the temperature increases accurately during these periods.

Conversely, La Niña events are typically associated with cooler-than-average temperatures, especially in the coastal areas. This cooling effect is due to the stronger-than-usual upwelling of cold, nutrient-rich water along the coast of Ecuador, which lowers the SST and subsequently the air temperature⁶⁹. In Figure 3.2 it is difficult to observe this effect, and in fact, for the RegCM5 simulation, there is no notable difference between El Niño and La Niña composites. Additionally, in the metrics registered in Table 3.1 for La Niña events, the model shows higher errors than those for El Niño and even than those for the Annual Mean, indicating significant discrepancies. Despite the higher errors, the Willmott Index and Pearson Correlation suggest that the model still captures the general cooling pattern, though with less accuracy. The median bias of 1.76°C indicates a warm bias, particularly along the coast where the cooling should be more significant than captured by the model.

3.1.2 Total Precipitation

Similarly, precipitation patterns in Ecuador are influenced by complex geographical and topographical factors. The coastal regions generally experience high annual precipitation, particularly during the rainy season, while the highlands and Amazon regions also receive substantial rainfall, though with

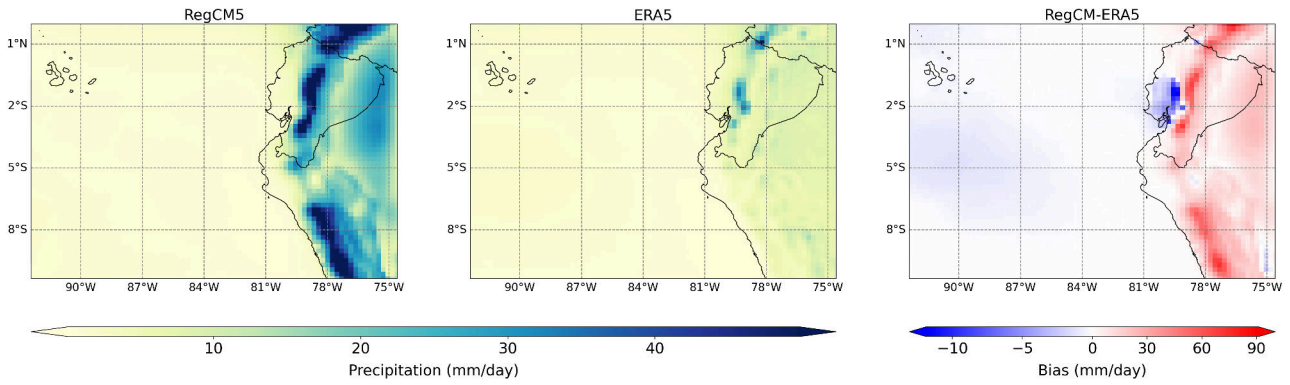


Figure 3.3: Annual mean total precipitation from RegCM5 simulation (left), ERA5 reanalysis data (middle), and the bias between them (right) for the period 1991-2020. The bias map highlights that the RegCM5 simulation overestimates precipitation in the central Andean region and the Amazon basin (shown in red), while it underestimates precipitation along the coastal region (shown in blue).

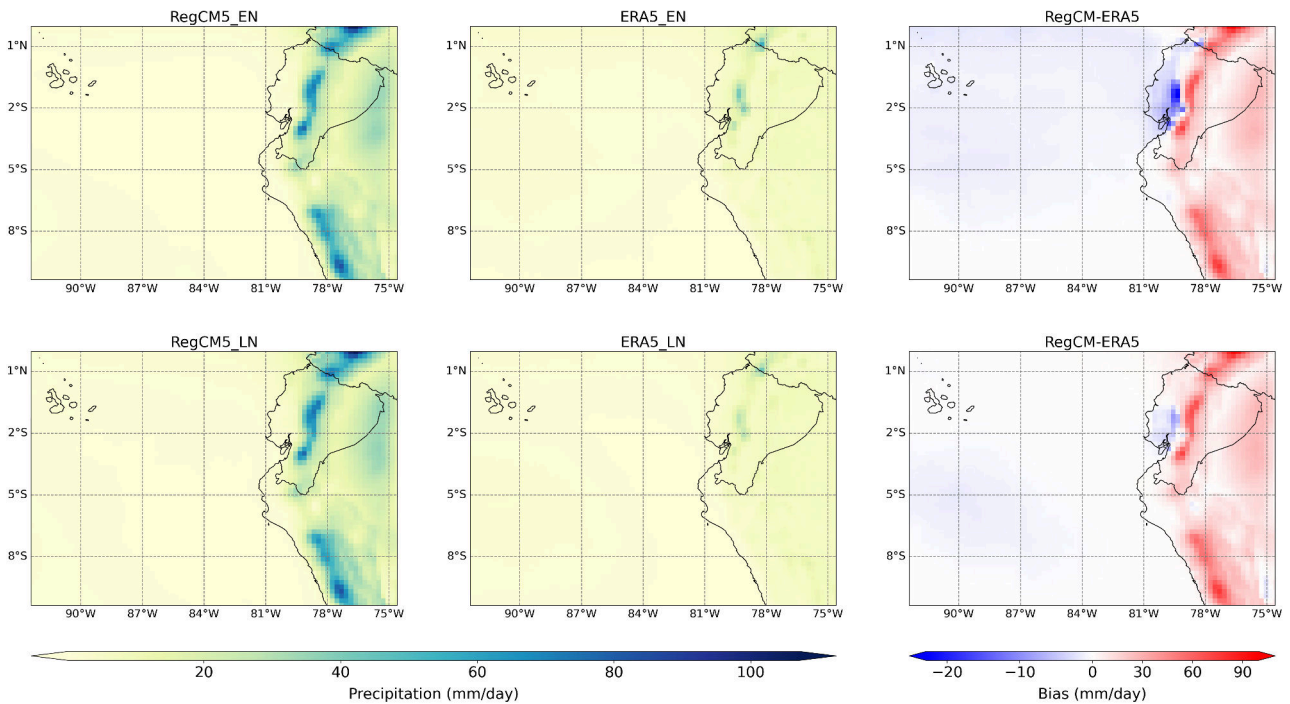


Figure 3.4: Composite total precipitation for El Niño (top row) and La Niña (bottom row) events from RegCM5 simulation (left), ERA5 reanalysis data (middle), and the bias between RegCM5 and ERA5 (right) for the period 1991-2020. During El Niño events, RegCM5 simulation overestimates precipitation in the Andean region and in some areas of the Amazon basin (shown in red), while underestimating the temperature along the Pacific coast (shown in blue). During La Niña events, the model continues to overestimate precipitation in the Andean and Amazon region, but also in some coastal areas (shown in red), while underestimating it in other coastal areas (shown in blue).

different seasonal distributions⁶⁶. In Figure 3.3 we can observe how the RegCM5 simulation failed to capture the general spatial distribution of precipitation across Ecuador. Particularly the model tends

Table 3.2: Error Metrics for Precipitation

Metric	Annual Mean	El Niño Event	La Niña Event
MAE (mm/day)	4.84	5.34	5.23
RMSE (mm/day)	11.16	11.67	11.90
Bias (mm/day)	-0.03	-0.42	0.11
Correlation	0.71	0.65	0.74
Willmott Index	0.53	0.50	0.51

to overestimate precipitation in the central Andean region and in the Amazon basin while underestimating it along the coastal region.

The metrics for annual mean precipitation in Table 3.2 reveal very high errors, although The Correlation Coefficient and the Willmott Index indicate moderate agreement between the RegCM5 simulation and the ERA5 data. These errors in precipitation modeling are common, primarily because precipitation is inherently challenging to simulate accurately. Numerous studies have documented these challenges, highlighting systematic biases and significant discrepancies in modeled precipitation across different regions and temporal scales^{42 70 71 72}.

The high spatial variability of precipitation in the Andes, driven by orographic effects, poses a challenge for models attempting to accurately depict localized precipitation patterns. The precipitation of Ecuador is particularly influenced by its varied topography and the interaction of different climatic systems. The coastal region is often dry due to the Humboldt Current, whereas the Andean region sees significant orographic precipitation owing to its elevation. Meanwhile, the Amazon basin experiences heavy rainfall year-round, influenced by moist air masses from the Atlantic Ocean²⁴. Orographic precipitation, a primary cause of rainfall in the Andes, results from the interaction of moist air with mountainous terrain. Accurately modeling this process is difficult because of the fine spatial scales and complex atmospheric dynamics involved¹⁸.

During El Niño events, characterized by warmer SSTs in the central and eastern Pacific, Ecuador generally experiences increased precipitation, particularly in the coastal and Amazon regions. This is due to the enhanced convection and moisture transport associated with the warm phase of ENSO⁶⁶. The RegCM5 simulation in Figure 3.4 captures this increase, but the comparison with ERA5 data shows significant discrepancies, as illustrated by the bias maps. The metrics in Table 3.2 endorse this, The errors for El Niño events are higher than the annual mean errors, reflecting the difficulty that the model has in accurately simulating the increased precipitation. The negative median bias of -0.42 mm/day suggests a slight tendency to underestimate precipitation during El Niño events. The

correlation coefficient and the Willmott Index indicate moderate agreement, but they highlight the need for better model performance during these extreme events.

Conversely, La Niña events are typically associated with decreased precipitation, particularly in the coastal areas, due to the stronger-than-usual upwelling of cold water along the coast, which reduces atmospheric convection and moisture availability⁶⁹. The RegCM5 simulation failed to capture the general pattern of reduced precipitation. In fact, similar to the El Niño events, shows notable discrepancies when compared to ERA5 data. The error metrics registered in Table 3.2 for La Niña events are slightly lower than those for El Niño events, but they still indicate significant deviations. The near-zero median bias of 0.11 mm/day suggests no significant overall bias in one direction, but the performance of the model varies across different regions. The correlation coefficient and the Willmott Index suggest that the model has slightly better agreement with observations during La Niña events compared to El Niño events, but there is still considerable room for improvement.

3.1.3 Divergence of Winds at 10m

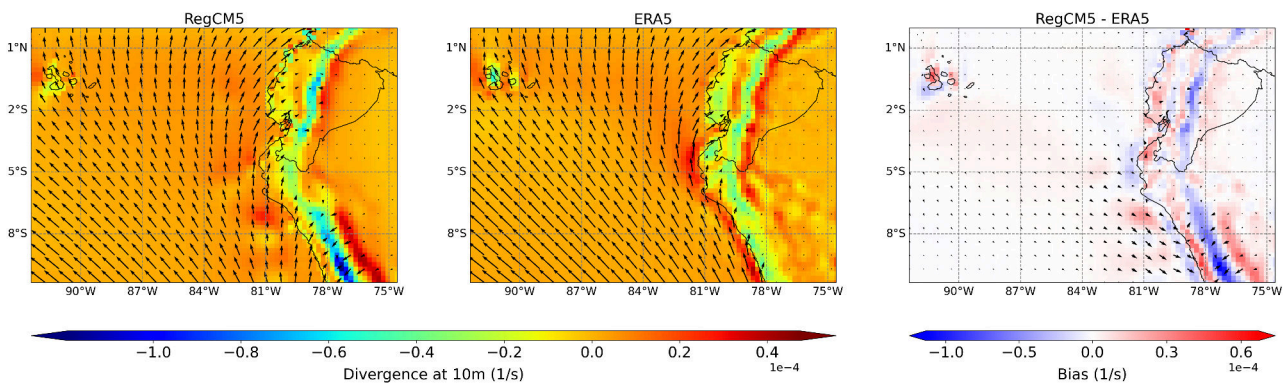


Figure 3.5: Annual mean wind divergence at 10m from RegCM5 simulation (left), ERA5 reanalysis data (middle), and the bias between them (right) for the period 1991-2020. The divergence is shown in 1/s and the arrows represent the direction and velocity of the winds. The bias map highlights areas where the RegCM5 simulation overestimates divergence, particularly in some areas of the coastal and Amazon regions (shown in red), and areas where it underestimates divergence, such as the Andean region (shown in blue).

Wind dynamics in Ecuador generally depend on the region. In coastal areas, strong westerly winds influenced by the Pacific Ocean are observed. In the Andes, wind patterns are much more variable and erratic due to the mountainous terrain. In the Amazon, winds are quite weak and also vary greatly, but due to the dense forest cover in the area⁴³.

Figure 3.5 illustrates the annual mean wind divergence at 10m. The RegCM5 simulation represents in general the patterns of the wind, but with some discrepancies. The metrics in Table3.3 reveal that

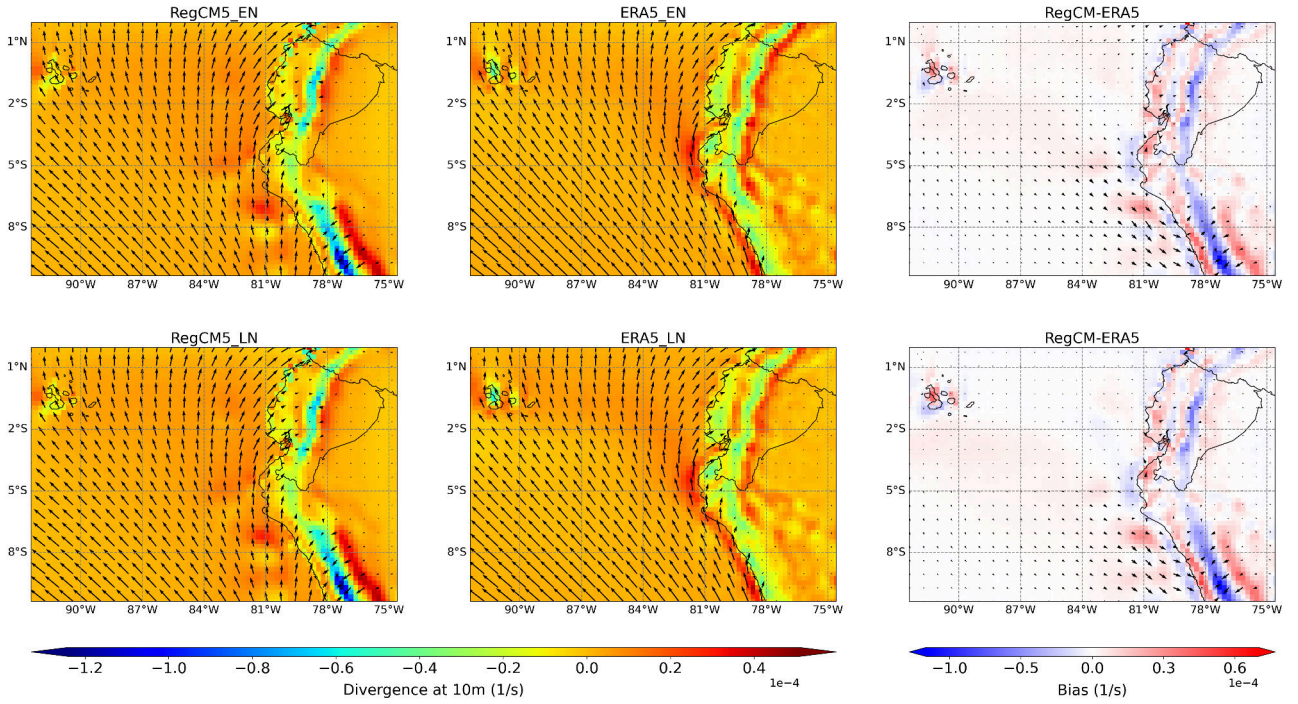


Figure 3.6: Composite wind divergence at 10m for El Niño (top row) and La Niña (bottom row) events from RegCM5 simulation (left), ERA5 reanalysis data (middle), and the bias between them (right) for the period 1991-2020. The divergence is shown in 1/s and the arrows represent the direction and velocity of the winds. During El Niño events, the RegCM5 simulation overestimates divergence along the coast and Amazon regions (shown in red), while underestimating it in the Andean region (shown in blue). During La Niña events, the model shows similar discrepancies.

Table 3.3: Error Metrics for Wind Divergence at 10m

Metric	Annual Mean	El Niño	La Niña
MAE (1/s)	4.9e-06	5.1e-06	5.1e-06
RMSE (1/s)	1.0e-05	1.1e-05	1.0e-05
Bias (1/s)	4.0e-07	8.5e-07	5.7e-07
Correlation	0.52	0.50	0.50
Willmott Index	0.68	0.66	0.66

the performance of the model in simulating wind divergence is moderate, with significant errors, particularly underestimating the divergence in the Andean region and overestimating it in the coast. The correlation coefficient and the Willmott Index indicate moderate agreement between the model and the ERA5, suggesting that while the model captures general patterns, significant discrepancies remain.

During El Niño events, Ecuador generally experiences changes in wind patterns, including increased divergence along the coast and Amazon region due to enhanced convection and moisture transport⁶⁶. In Figure 3.6 the RegCM5 simulation captures some aspects of these changes, but the comparison with ERA5 data reveals some discrepancies, particularly in the magnitude of divergence.

The metrics for El Niño events in Table 3.3 show errors slightly higher than the annual mean ones, reflecting how challenging it is for the model to accurately simulate these dynamic conditions. The correlation coefficient and the Willmott Index indicate moderate agreement and the bias of 8.5×10^{-7} 1/s suggests a tendency to overestimate divergence during El Niño events.

Conversely, La Niña events, typically result in decreased wind divergence, particularly along the coast. This reduction is due to the stronger-than-usual upwelling of cold water, which stabilizes the atmosphere and reduces convection⁶⁹. The RegCM5 simulation in Figure 3.6 failed to capture the pattern of reduced divergence. In fact, the graphs for El Niño and La Niña events are very similar for the RegCM5 simulation. Although the difference between these same graphs with the ERA5 data is not very noticeable either, we can observe a slightly higher divergence in the Andean region, which will be more visible at higher altitudes. The metrics for La Niña events show similar errors than those for El Niño events but still indicate notable deviations. The correlation coefficient and the Willmott Index show that while the model captures the general trend, there is considerable room for improvement to accurately represent the reduced divergence during La Niña events. The median bias of 5.7×10^{-7} 1/s suggests a slight overestimation of divergence.

3.1.4 Divergence of Winds at 100m

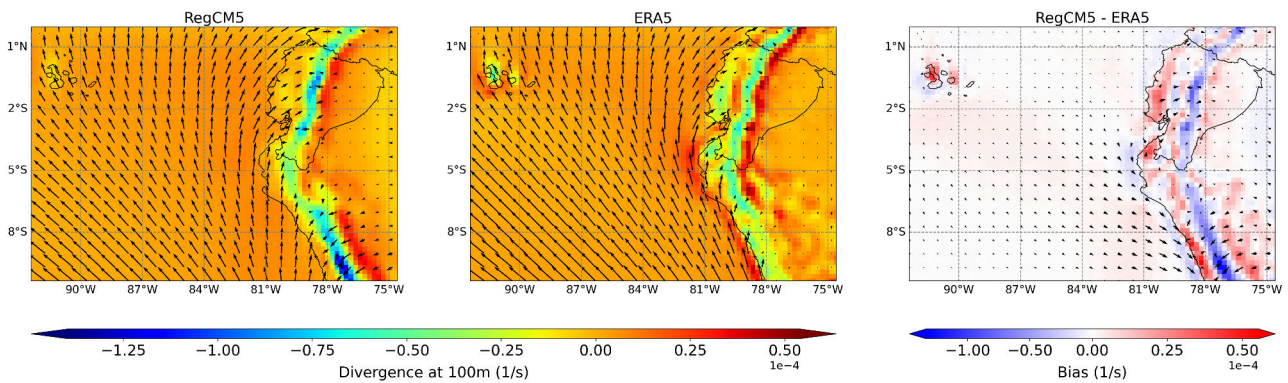


Figure 3.7: Annual mean wind divergence at 100m from RegCM5 simulation (left), ERA5 reanalysis data (middle), and the bias between them (right) for the period 1991-2020. The divergence is shown in 1/s and the arrows represent the direction and velocity of the winds. The bias map highlights areas where the RegCM5 simulation overestimates divergence, particularly along the coastal regions and parts of the Amazon basin (shown in red), and areas where it underestimates divergence, such as the Andean region (shown in blue).

The wind patterns at 100 meters above the surface in Ecuador are generally more influenced by broader atmospheric circulation and less by immediate surface features compared to winds at 10 meters. At 100 meters, the winds tend to be more consistent and less variable due to the reduced

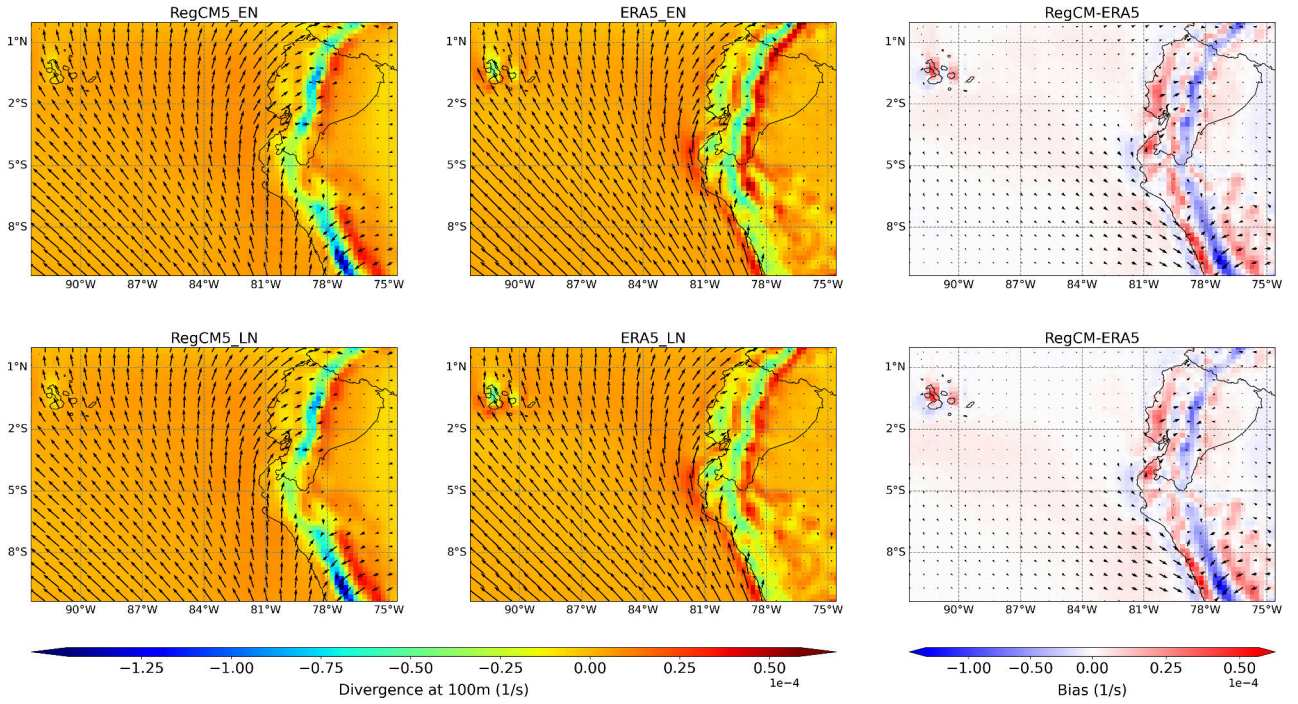


Figure 3.8: Composite wind divergence at 100m for El Niño (top row) and La Niña (bottom row) events from RegCM5 simulation (left), ERA5 reanalysis data (middle), and the bias between them (right) for the period 1991-2020. The divergence is shown in 1/s and the arrows represent the direction and velocity of the winds. During El Niño events, the RegCM5 simulation overestimates divergence in the coastal and Amazon regions (shown in red), while underestimating it in the Andean region (shown in blue). During La Niña events, the model shows similar discrepancies.

Table 3.4: Error Metrics for Wind Divergence at 100m

Metric	Annual Mean	El Niño	La Niña
MAE (1/s)	5.4e-06	6.0e-06	5.5e-06
RMSE (1/s)	1.2e-05	1.2e-05	1.2e-05
Bias (1/s)	5.5e-07	1.0e-06	7.3e-07
Correlation	0.56	0.53	0.55
Willmott Index	0.73	0.70	0.70

frictional influence of the surface⁴³.

Figure 3.7 illustrates the annual mean wind divergence at 100m, showing that the RegCM5 simulation represents the general patterns, but with discrepancies similar to those observed at 10 meters. The metrics in Table 3.4 reveal that the performance of the model in simulating wind divergence at 100 meters is moderate, with lower errors than at 10 meters. The correlation coefficient and the Willmott Index suggest moderate agreement between the model and the ERA5 data, though significant discrepancies remain. The median bias of 5.5×10^{-7} 1/s indicates a slight overestimation, similar to the pattern observed at 10 meters.

During El Niño and La Niña events, the wind divergence at 100 meters shows changes similar to those at 10 meters but with less pronounced local variations and more pronounced large-scale patterns. The increased divergence during El Niño and decreased divergence during La Niña reflect the altered atmospheric circulation associated with these events, affecting broader regions more uniformly at 100 meters compared to 10 meters⁴³.

In Figure 3.8 we can observe that the RegCM5 simulation captures some aspects of the increased divergence due to enhanced convection and moisture transport, particularly in the coastal and Amazon regions. However, the comparison with ERA5 data reveals substantial discrepancies in the magnitude and spatial distribution of divergence. The metrics for El Niño events in Table 3.4 show higher errors than the annual mean, reflecting the challenges in accurately simulating these dynamic conditions with this model. The correlation coefficient and the Willmott Index indicate moderate agreement, while the bias of 1.0×10^{-6} 1/s suggests a tendency to overestimate divergence during El Niño events.

Conversely, La Niña events, characterized by reduced divergence due to stronger-than-usual upwelling of cold water, show similar discrepancies in the RegCM5 simulation at 100 meters. The model struggles to capture the reduced divergence accurately, as shown in Figure 3.8. The metrics for La Niña events reveal high errors, indicating significant deviations from ERA5 data. The correlation coefficient and the Willmott indicate moderate agreement, but the performance of the model needs improvement to accurately represent the reduced divergence during La Niña events. The bias of 7.3×10^{-7} 1/s suggests a slight overestimation, similar to the pattern observed at 10 meters, which suggests that this is a systematic bias.

These discrepancies in modeling wind divergence could be closely related to the difficulties of the model in accurately simulating precipitation patterns. Wind divergence is a key factor in the formation of clouds and precipitation. Errors in wind divergence can lead to inaccuracies in representing the vertical motion of air, which is crucial for cloud formation and precipitation processes. For instance, overestimating wind divergence in the coastal regions and underestimating it in the Andean regions can result in incorrect precipitation estimates, as seen in the precipitation analysis⁷¹.

3.1.5 Specific Humidity

Similarly, specific humidity in Ecuador also varies between different regions. For example, the coastal and Amazonian regions have high specific humidity, the coast due to its proximity to large bodies of water, and the Amazon due to its dense vegetation. On the other hand, the Andes tend to have lower specific humidity due to their higher altitude and cooler temperatures²⁴. For this study, we

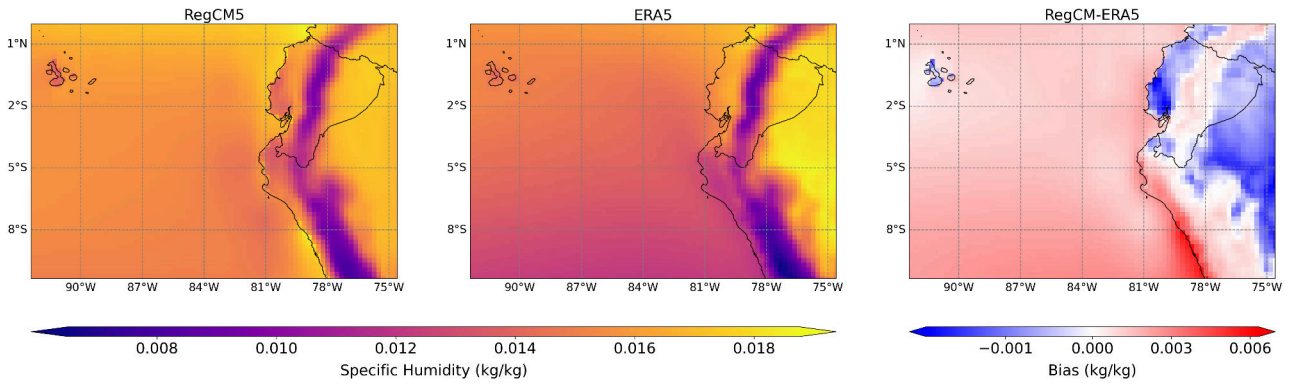


Figure 3.9: Annual mean specific humidity from RegCM5 simulation (left), ERA5 reanalysis data (middle), and the bias between them (right) for the period 1991-2020. The bias map highlights areas where the RegCM5 simulation underestimates specific humidity, particularly in the Amazon region, along the coast, and in the insular region (shown in blue), and areas where it overestimates specific humidity, such as the Andean region (shown in red).

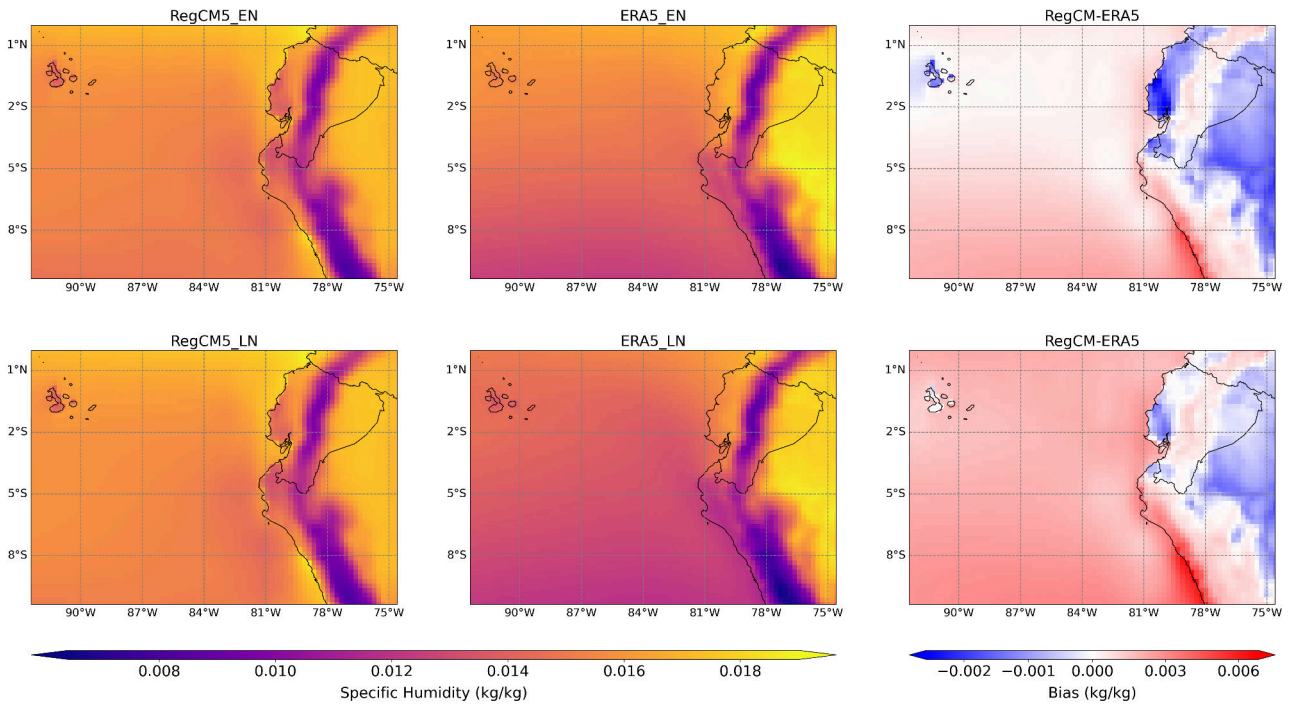


Figure 3.10: Composite specific humidity for El Niño (top row) and La Niña (bottom row) events from RegCM5 simulation (left), ERA5 reanalysis data (middle), and the bias between them (right) for the period 1991-2020. During El Niño events, the RegCM5 simulation underestimates specific humidity in the Amazon region, along the coast, and in the insular region (shown in blue), while overestimating it in the Andean region (shown in red). During La Niña events, the model shows similar discrepancies but with less magnitude.

calculate specific humidity as the ratio of the mass of water vapor to the total mass of air (including water vapor) and use the unit kg/kg, which expresses the mass of water vapor per unit mass of air⁷³.

Table 3.5: Error Metrics for Specific Humidity

Metric	Annual Mean	El Niño Event	La Niña Event
MAE (kg/kg)	1.4×10^{-3}	9.7×10^{-4}	1.8×10^{-3}
RMSE (kg/kg)	1.6×10^{-3}	1.2×10^{-3}	2.0×10^{-3}
Bias (kg/kg)	1.2×10^{-3}	4.7×10^{-4}	1.9×10^{-3}
Correlation	0.83	0.86	0.80
Willmott Index	0.83	0.89	0.76

The RegCM5 simulation in Figure 3.9 captures the overall distribution of specific humidity across Ecuador but shows slight discrepancies in certain regions. The bias maps indicate that the model tends to underestimate specific humidity in the Amazon region and along the coast while overestimating it in the Andean region. The metrics in Table 3.5 indicate that the RegCM5 simulation exhibits small errors, suggesting that the model reasonably captures the spatial variability of specific humidity, and the bias of 1.2×10^{-3} kg/kg suggests that the model consistently overestimates the values. The high correlation coefficient and the Willmott Index also indicate a good agreement between the model and ERA5 data, despite the biases.

During El Niño events, specific humidity generally increases, especially in the coastal and Amazon regions, due to enhanced convection and moisture transport from the warmer ocean surfaces⁶⁶. The RegCM5 simulation relatively captures this increase in specific humidity during El Niño events, but it failed in terms of magnitude. The metrics for El Niño events in Table 3.5 show lower errors compared to the annual mean and the higher correlation coefficient and the Willmott Index suggesting that the model performs well in capturing the increased specific humidity during El Niño events. However, the median bias of 4.7×10^{-4} kg/kg suggests a slight overestimation.

Conversely, La Niña events are associated with decreased specific humidity, particularly in the coastal regions, due to stronger upwelling of cold water and reduced atmospheric convection⁶⁹. The RegCM5 model shows more significant discrepancies during La Niña events. The error metrics for La Niña events in Table 3.5 reveal higher errors compared to El Niño events, along with a moderate correlation coefficient and Willmott Index suggest moderate agreement, but the performance of the model is less accurate compared to El Niño events. The bias of 1.9×10^{-4} kg/kg indicates a substantial overestimation of specific humidity during La Niña events.

3.1.6 Relative Humidity

Relative humidity in Ecuador, like specific humidity, varies significantly across different regions due to the country's diverse topography and climatic influences. Coastal and Amazon regions generally exhibit higher relative humidity because of their proximity to large water bodies and dense vegetation, which contribute to high moisture content in the air. In contrast, the Andean highlands tend to have lower relative humidity due to their higher altitudes and cooler temperatures, which reduce the capacity of air masses to hold moisture²⁴. Relative humidity is a percentage that indicates how close the air is to saturation, depending on both the moisture content and air temperature. In contrast, specific humidity measures the actual moisture content in the air, independent of temperature⁷³.

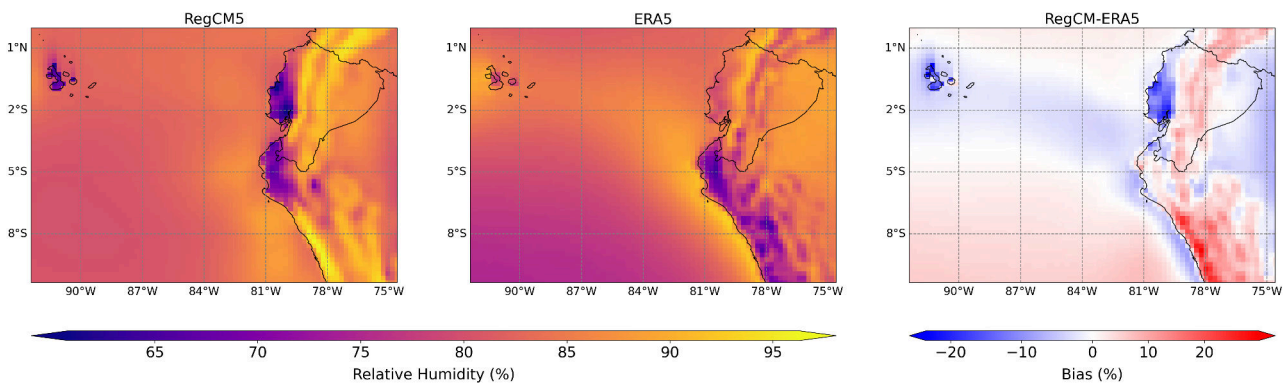


Figure 3.11: Annual mean relative humidity from RegCM5 simulation (left), ERA5 reanalysis data (middle), and the bias between them (right) for the period 1991-2020. The bias map shows that the RegCM5 simulation underestimates relative humidity along the coast and some parts of the Amazon region (shown in blue) while overestimating it in the Andean region (shown in red).

The RegCM5 simulation in Figure 3.11 captures the general spatial distribution of relative humidity across Ecuador but with notable discrepancies. The bias maps reveal that the model tends to underestimate relative humidity along the coast and some parts of the Amazon region while overestimating it in the Andean region. The metrics in Table 3.6 indicate that the RegCM5 simulation exhibits moderate errors and the medium correlation coefficient and the Willmott Index suggest a moderate agreement between the model and ERA5 data, despite these biases. Additionally, a bias of 0.81% suggests a general overestimation of the relative humidity.

Table 3.6: Error Metrics for Relative Humidity

Metric	Annual Mean	El Niño Event	La Niña Event
MAE (%)	3.34	3.22	3.28
RMSE (%)	4.68	4.63	4.68
Bias (%)	0.81	0.89	0.79
Correlation	0.42	0.43	0.42
Willmott Index	0.65	0.64	0.65

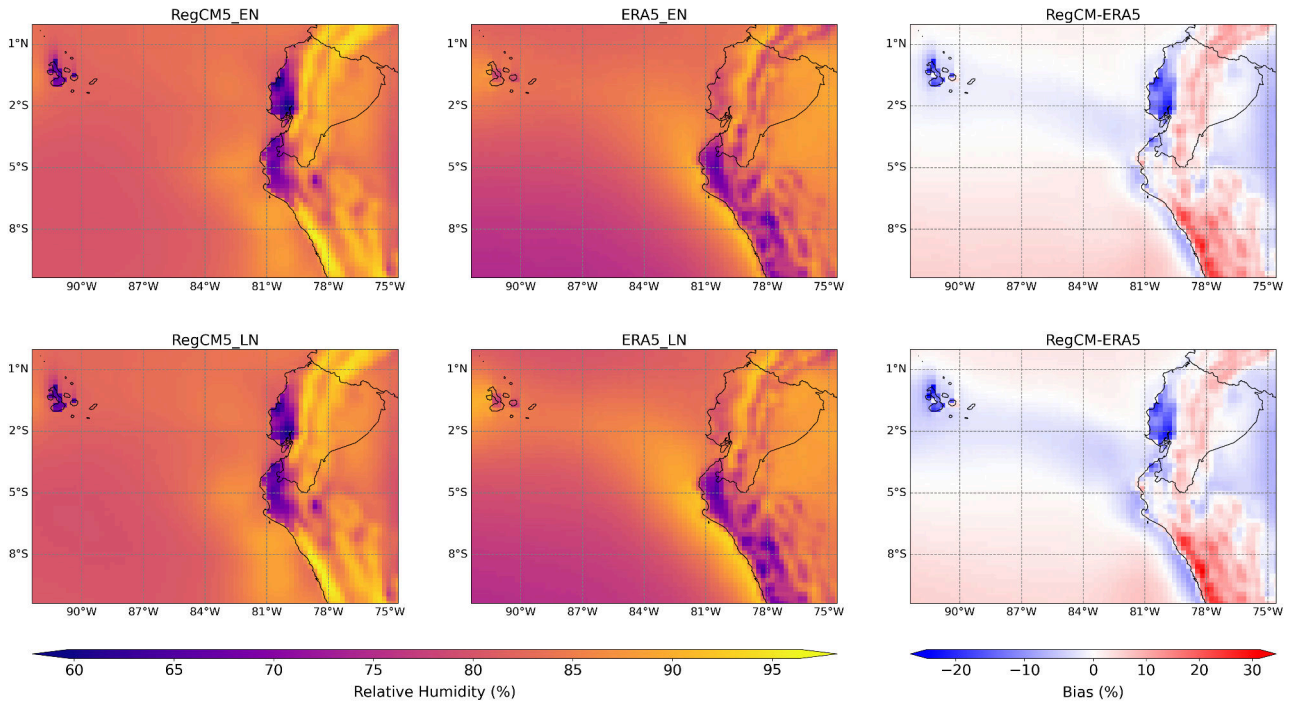


Figure 3.12: Composite relative humidity for El Niño (top row) and La Niña (bottom row) events from RegCM5 simulation (left), ERA5 reanalysis data (middle), and the bias between them (right) for the period 1991-2020. During El Niño events, RegCM5 simulation generally underestimates relative humidity in coastal and Amazon regions (shown in blue), while overestimating it in the Andean region (shown in red). During La Niña events, the model shows very similar discrepancies.

During El Niño events, relative humidity typically increases, especially in the coastal and Amazon regions, due to enhanced convection and moisture transport from the warmer ocean surfaces⁶⁶. The RegCM5 simulation captures this increase in relative humidity during El Niño events but with varying accuracy. The metrics for El Niño events in Table 3.6 show errors similar to the annual mean, with slightly better performance indicated by a higher correlation coefficient and the Willmott Index. However, the bias of 0.89% suggests a slight overestimation of relative humidity during these events.

Conversely, La Niña events are associated with decreased relative humidity, particularly in the coastal regions⁶⁹. The RegCM5 simulation shows discrepancies during La Niña events similar to those observed during El Niño events. The error metrics for La Niña events in Table 3.6 reveal higher errors compared to El Niño events, along with a moderate correlation coefficient and the Willmott Index. The bias of 0.79% indicates a slight overestimation of relative humidity during La Niña events. It is important to note that the correlation and the Willmott Index are higher for specific humidity compared to relative humidity primarily because specific humidity is more stable and less sensitive to temperature variations. In contrast, relative humidity is a percentage that depends heavily on temperature, making it more variable and sensitive to errors in both temperature and specific humidity.

Notably, areas where the model overestimates relative humidity values, also present large amounts of precipitation. This result is more marked over the Andean region and coincides with the tendency of RegCM5 to overestimate specific and relative humidity. This may lead to predicted precipitation that does not correspond to observed values. However, the model predicts low levels of precipitation for the coastal region which are consistent with the observations.

3.2 Bias Correction

Given the discrepancies identified in the validation of the RegCM5 simulation, a bias correction has been applied to the monthly data of these variables to improve the accuracy of the model simulations, particularly for near-surface air temperature and precipitation. These variables are crucial due to their significant influence on, and sensitivity to, the El Niño-Southern Oscillation (ENSO). The Quantile Delta Mapping bias correction aims to mitigate systematic errors and enhance the ability of the model to capture the spatial and temporal variability of these key climatic variables.

For this analysis, the data were divided into two periods: the calibration period (1991-2010) and the validation period (2011-2020). The following sections present the results of the bias correction for annual mean values and ENSO-related composites (El Niño and La Niña events) for the validation period.

3.2.1 Near-Surface Air Temperature

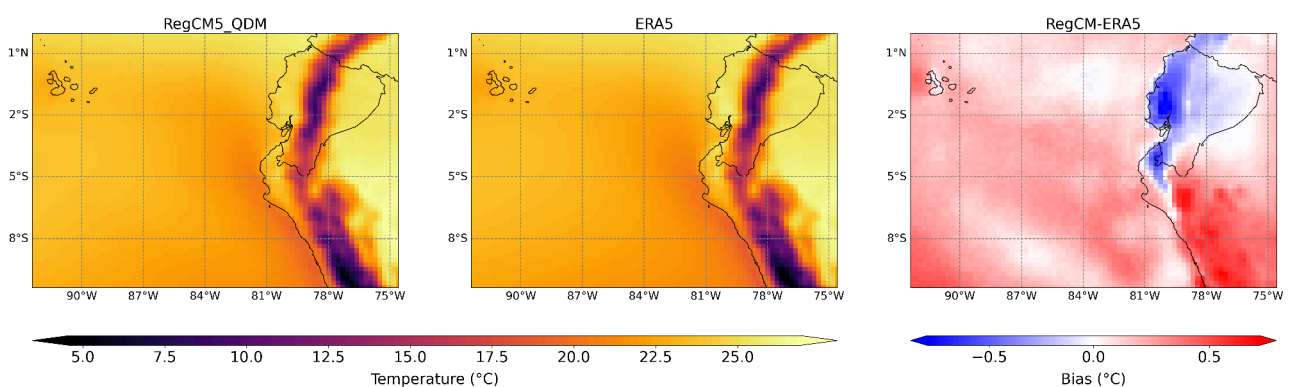


Figure 3.13: Annual mean near-surface air temperature from RegCM5 simulation with bias correction (left), ERA5 reanalysis data (middle), and the bias between them (right) for the period 2011-2020. The bias map highlights areas where the RegCM5 simulation underestimates temperatures, particularly throughout continental Ecuador (shown in blue).

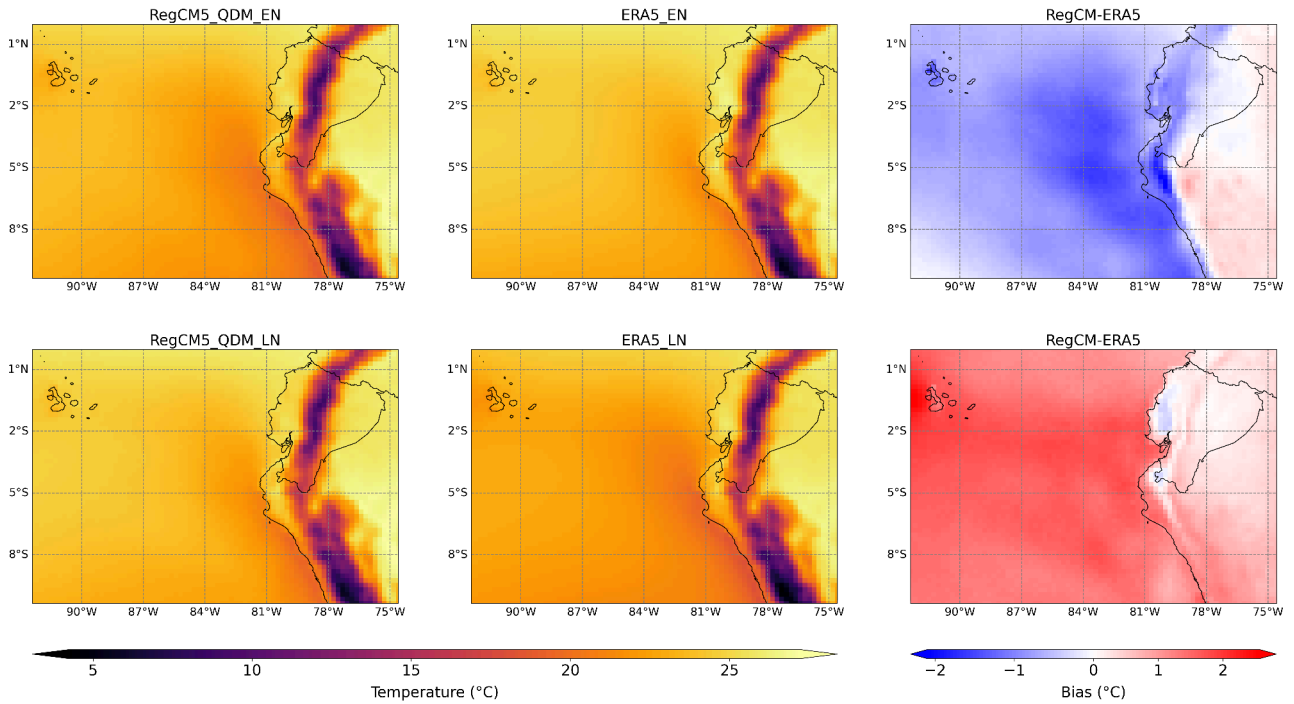


Figure 3.14: Composite near-surface air temperature for El Niño (top row) and La Niña (bottom row) events from RegCM5 simulation with bias correction (left), ERA5 reanalysis data (middle), and the bias between them (right) for the period 2011-2020. During El Niño events, RegCM5 simulation underestimates temperatures along the Pacific coast, the insular, and Andean region (shown in blue), while overestimating temperatures in some areas of the Amazon basin (shown in red). During La Niña events, the model overestimates temperatures in the Andes, as well as in some areas of the Amazon region (shown in red), while underestimating temperatures in some coast areas (shown in blue).

Table 3.7: Error Metrics for Near-Surface Air Temperature with and without Bias Correction

Event	MAE	RMSE	Bias	Correlation	Willmott Index
Annual Mean					
Corrected	0.21	0.25	0.18	1.00	1.00
Original	1.17	1.40	1.06	0.95	0.96
El Niño Event					
Corrected	0.68	0.79	-0.69	0.99	0.99
Original	0.53	0.83	0.08	0.97	0.98
La Niña Event					
Corrected	1.17	1.28	1.33	0.99	0.96
Original	1.95	2.25	2.32	0.92	0.90

The application of bias correction to the RegCM5 simulation significantly improves the accuracy of near-surface air temperature simulations for the period 2011-2020. In Figure 3.13 we can observe that the bias correction markedly reduces the systematic warm bias that the original model exhibited across most regions of Ecuador, particularly in coastal and Andean areas. The corrected model

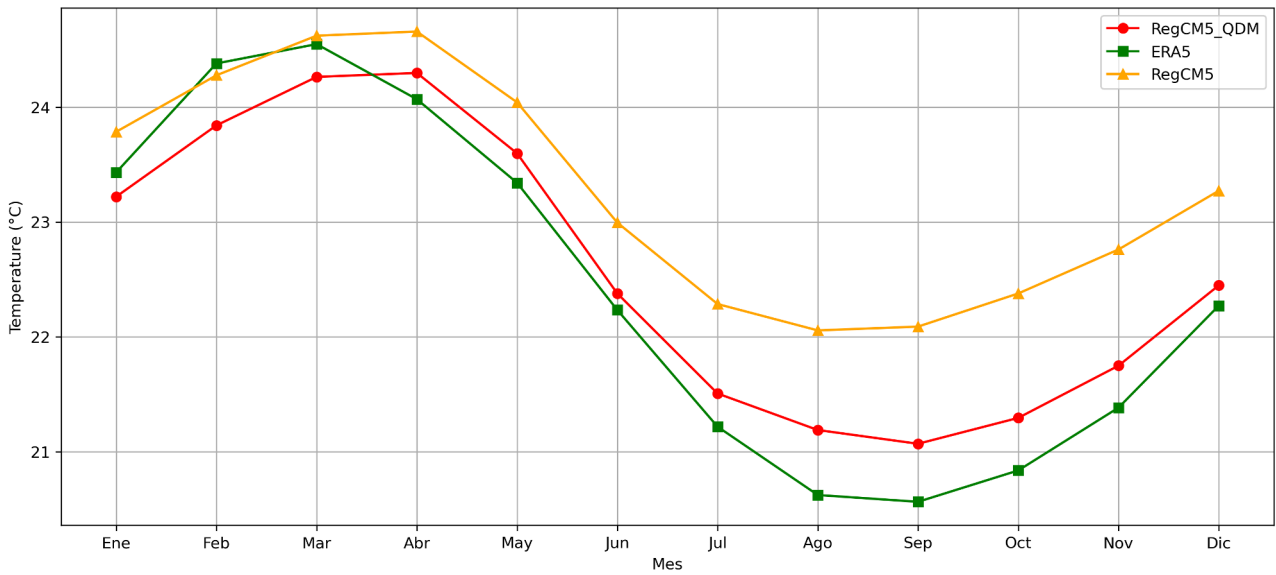


Figure 3.15: Annual Cycle of near-surface air temperature for the period 2011-2020. The bias-corrected model (RegCM5_QDM) aligns more closely with ERA5 data, particularly during the cooler months from July to December, reducing the overall error and improving the representation of seasonal temperature variations in Ecuador.

(RegCM5_QDM) also decreases this warm bias, bringing the temperature estimates much closer to the ERA5 reanalysis data. The metrics in Table 3.7 indicate that the corrected model eliminates most overestimations, achieving a reduction in the Mean Absolute Error (MAE) from 1.17°C to 0.21°C and the Root Mean Square Error (RMSE) from 1.40°C to 0.25°C . Additionally, the systematic bias decreases from 1.06°C to 0.18°C , and the correlation coefficient significantly improves from 0.95 to 0.99, indicating an almost perfect alignment with the ERA5 data. The Willmott Index also improves from 0.96 to 0.99, suggesting better agreement between the model and observations.

In Figure 3.14, we can observe a clear distinction between El Niño and La Niña events, highlighting the different patterns in near-surface air temperature associated with each event. During El Niño events, the original model captures the general pattern of increased temperatures with a small underestimation in coastal regions. Despite the application of the bias correction, the corrected model (RegCM5_QDM) shows an increase in MAE from 0.53°C to 0.68°C , indicating a slight increase in error. Although the RMSE decreases from 0.83°C to 0.79°C , showing some improvement in overall error magnitude, the bias shifts direction to -0.69°C , indicating a slight underestimation after correction. The correlation coefficient improves slightly from 0.97 to 0.99, and the Willmott Index remains high, indicating good model performance.

During La Niña events, the original model presents a strong warm bias with a significant over-

estimation of temperature. The corrected model shows a substantial reduction in bias, although some overestimation persists. The metrics show notable improvement: MAE reduces from 1.95°C to 1.17°C, and RMSE from 2.25°C to 1.28°C. The bias decreases from 2.3°C to 1.33°C, showing a substantial correction of the original warm bias of the model. The correlation coefficient improves from 0.92 to 0.99, and the Willmott Index increases from 0.90 to 0.96, indicating a much better alignment with the ERA5 data for La Niña Events.

Through this validation, it is demonstrated that the QDM bias correction significantly improves the results for surface air temperature. In fact, it can be observed in the analyses of the annual means and ENSO events that the adjustments to the estimates have notably decreased the errors previously recorded. Additionally, the annual temperature cycle shown in Figure 3.15 underlines this statement. We can see how the original model overestimated temperatures compared to the ERA5 data, particularly during the colder months from July to December. On the other hand, the corrected model shows a much better fit to the ERA5 data throughout the year.

3.2.2 Total Precipitation

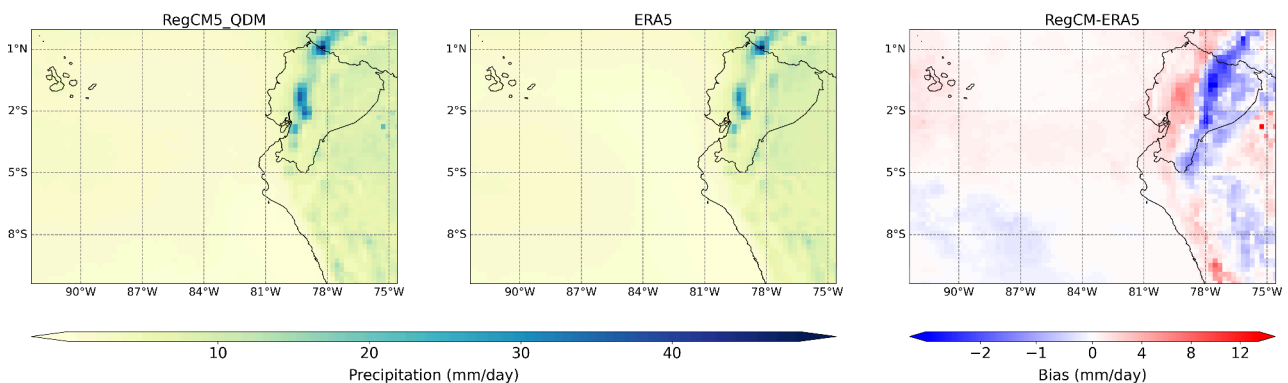


Figure 3.16: Annual mean precipitation from RegCM5 simulation data corrected (left), ERA5 re-analysis data (middle), and the bias between them (right) for the period 2011-2020. The bias map highlights areas where the RegCM5 simulation overestimates precipitation, particularly along the Pacific coast and some areas of the Andean region (shown in red), while overestimating precipitation in the Amazon region (shown in blue).

The application of bias correction to the RegCM5 simulation significantly improves the accuracy of precipitation simulations for the period 2011-2020. In Figure 3.16, the corrected model (RegCM5_QDM) shows a substantial reduction in both systematic biases and random errors when compared to the original model. The annual mean precipitation analysis indicates that the corrected model effectively reduces the systematic bias observed in the original model, particularly in the coastal region where precipitation is typically high. The error metrics highlight these improvements, with

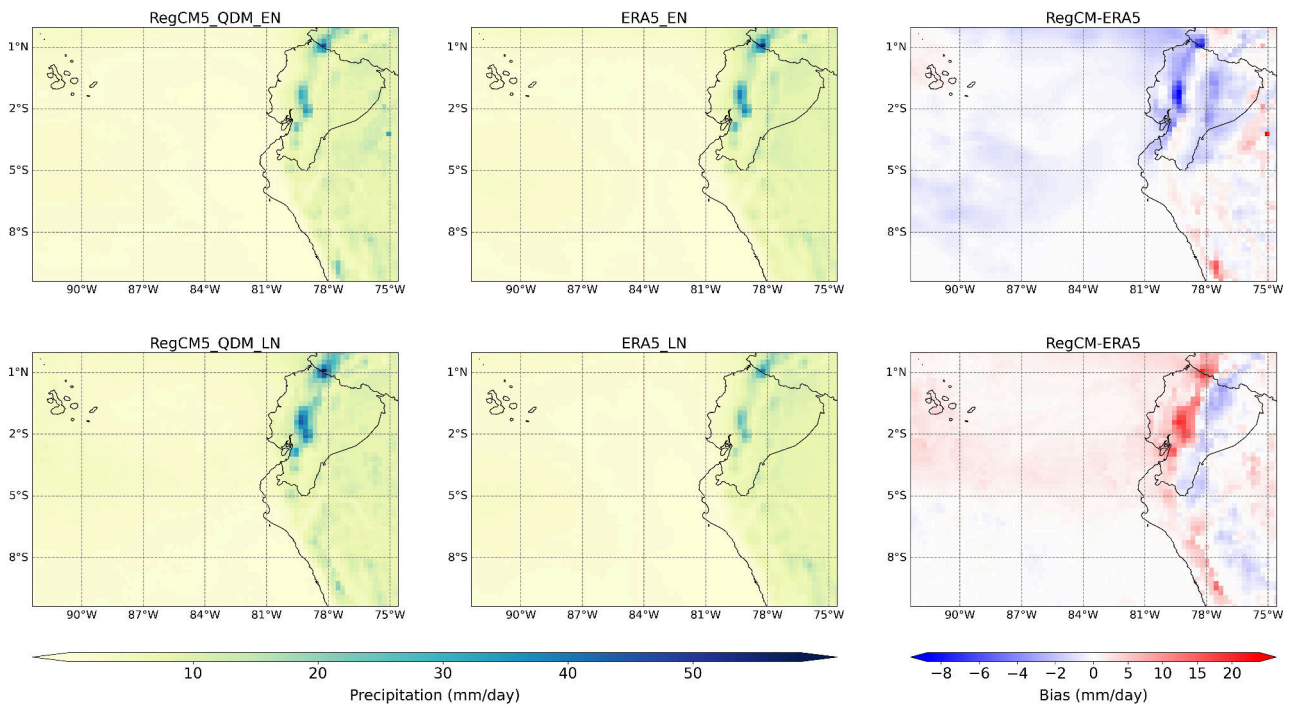


Figure 3.17: Composite precipitation for El Niño (top row) and La Niña (bottom row) events from RegCM5 simulation data corrected (left), ERA5 reanalysis data (middle), and the bias between them (right) for the period 2011-2020. During El Niño events, RegCM5 simulation underestimates precipitations along the Pacific coast and in the Amazon basin (shown in blue). During La Niña events, the model overestimates precipitations in the coast region, as well as in some areas of the Andean region (shown in red), while underestimating temperatures in the Amazon basin (shown in blue).

Table 3.8: Error Metrics for Precipitation with and without Bias Correction

Event	MAE	RMSE	Bias	Correlation	Willmott Index
Annual Mean					
Corrected	0.56	0.96	0.24	0.98	0.99
Original	4.9	11	0.12	0.71	0.52
El Niño Event					
Corrected	0.62	1.2	-0.23	0.96	0.98
Original	5.7	13	-0.27	0.66	0.50
La Niña Event					
Corrected	1.2	2.2	0.63	0.92	0.93
Original	6.0	13	0.56	0.75	0.47

the MAE decreasing from 4.88 mm/day to 0.56 mm/day and the RMSE from 11.42 mm/day to 0.96 mm/day. The bias shows a slight increase from 0.12 mm/day to 0.24 mm/day, indicating minor overestimation. The correlation coefficient improves significantly from 0.71 to 0.98, demonstrating a stronger alignment with ERA5 data, and the Willmott Index increases from 0.52 to 0.98, indicating better model performance overall.

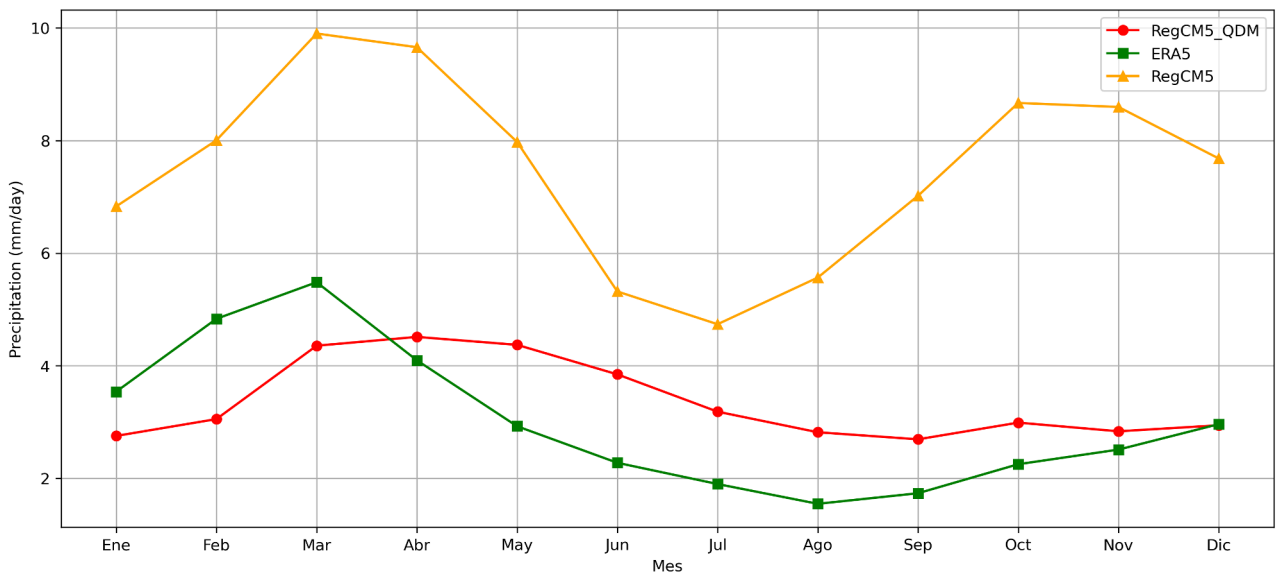


Figure 3.18: Annual Cycle of total precipitation for the period 2011-2020. The original model (RegCM5) consistently overestimates precipitation throughout the year compared to ERA5 data, with a pronounced peak during the wet season. The corrected model (RegCM5_QDM) aligns much more closely with ERA5. This alignment reduces the overall error and provides a more accurate representation of the seasonal precipitation variation in Ecuador.

In Figure 3.17, we can observe the distinction between El Niño and La Niña events in terms of precipitation patterns. During El Niño events, the original model tends to overestimate precipitation significantly, especially in the Andean regions. The corrected model aligns more closely with ERA5 data, reducing the MAE from 5.65 mm/day to 0.62 mm/day and the RMSE from 12.78 mm/day to 1.17 mm/day. The bias shows a slight improvement, shifting from -0.27 mm/day to -0.23 mm/day. The correlation coefficient improves from 0.66 to 0.96, and the Willmott Index from 0.50 to 0.98, indicating enhanced model performance post-correction.

For La Niña events, the original model exhibits a strong overestimation of precipitation, which is significantly corrected in the RegCM5_QDM model. The corrected model shows a marked improvement in error metrics, with the MAE decreasing from 5.98 mm/day to 1.21 mm/day and the RMSE from 13.47 mm/day to 2.20 mm/day. The bias increases slightly from 0.56 mm/day to 0.63 mm/day, indicating a small overestimation. The correlation coefficient improves from 0.75 to 0.92, and the Willmott Index increases from 0.47 to 0.93, demonstrating a better agreement with ERA5 data for La Niña events.

Overall, the improvement of the model is much more notable for the precipitation variable, since once the bias correction is applied, a significant reduction in errors especially in the spatial distribution

of precipitation can be observed, which was previously too far from the ERA5 data. This improvement can also be observed in the El Niño and La Niña events, which, despite showing stronger precipitation during La Niña than El Niño, which is a bit far from reality, still considerably increases the precision and therefore the confidence in the results. Additionally, the annual precipitation cycle, shown in Figure 3.18, shows a very significant improvement, since the original model (RegCM5) tended to greatly overestimate precipitation throughout the year compared to the ERA5 data, especially during the wet season. However, the corrected model (RegCM5_QDM) fits the ERA5 data much better, particularly in the wettest months from February to May. Therefore, we can say that the bias correction improved the temporal variability of precipitation, as well as its spatial distribution, which gives us a much more accurate representation of this variable.

3.3 Identification of El Niño and La Niña Events

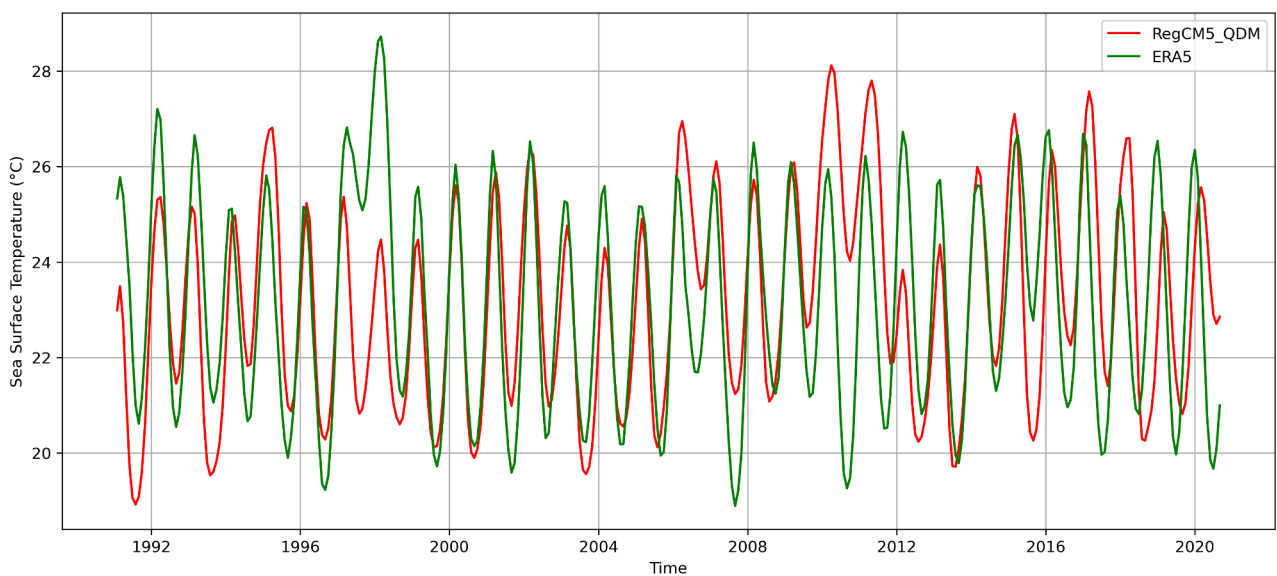


Figure 3.19: Three-month running mean of the Sea Surface Temperature of the El Niño 1+2 Region for the period 1991-2020

Table 3.9: Comparison of ENSO Event Counts for the period 1991-2020.

Data Source	El Niño Events	La Niña Events
ONI	9	10
RegCM5_QDM	11	12
ERA5	14	11

The identification of El Niño and La Niña events is a critical aspect of understanding climate variability and its impacts. In this analysis, the bias-corrected sea surface temperature (SST) data

from the RegCM5 model corrected (RegCM5_QDM) in the El Niño 1+2 Region was used to identify these events over the entire simulation period for the present (1991-2020) and near-future (2020-2050). Figure 3.19 illustrates the three-month running mean of SST from the bias-corrected RegCM5 model compared with ERA5 reanalysis data for the El Niño 1+2 Region. The close alignment between the corrected model and ERA5 indicates the effectiveness of the bias correction in capturing the temporal variability of SST.

Using the Oceanic Niño Index (ONI) thresholds and data from NOAA, we counted the number of El Niño and La Niña events for reference. The ONI identifies 9 El Niño events and 10 La Niña events. Applying the ICEN thresholds to the bias-corrected RegCM5_QDM data, we found 11 El Niño events and 12 La Niña events. In comparison, the ERA5 reanalysis data identifies 14 El Niño events and 11 La Niña events. These counts are summarized in Table 3.9.

The results obtained reveal slight discrepancies in the number of ENSO events identified by the different data sources. The ONI, which is used as a reference, recognizes a total of 19 events, while the bias-corrected RegCM5_QDM data identifies 23 events, and the ERA5 reanalysis data identifies 25 events. These differences highlight the uncertainties inherent in the detection of ENSO events and, above all, demonstrate that it is still a challenge to identify these events from a region other than the standard El Niño 3.4.

However, the close number of events identified by the bias-corrected RegCM5_QDM data compared to the ERA5 reanalysis data suggests that the bias correction has effectively improved the ability of the model to capture ENSO events. The small differences in event counts can be attributed to the different thresholds and data used for event classification. Despite not being a perfect method, this approach is acceptable for the classification of El Niño and La Niña events. The alignment between the corrected model data and the ERA5 reanalysis data provides confidence in the use of this method for detecting ENSO events. Therefore, it is suitable for identifying future El Niño and La Niña events allowing for relatively reliable climate projections of these events.

Using the same methodology for the identification of El Niño and La Niña events for the present period, we count the El Niño and La Niña events for the near-future RegCM5 simulation data, which identify 14 El Niño events and 10 La Niña events. These results align with other predictions that suggest El Niño events are going to increase while La Niña events are expected to decrease. Previous studies indicate that this trend is due to climate change, which is expected to increase the frequency and intensity of El Niño events due to higher sea surface temperatures in the central and eastern Pacific Oceans. This shift is attributed to changes in atmospheric circulation patterns and ocean-atmosphere interactions under global warming scenarios^{74,75}.

3.4 Near-Future Projections

3.4.1 Near-Surface Air Temperature

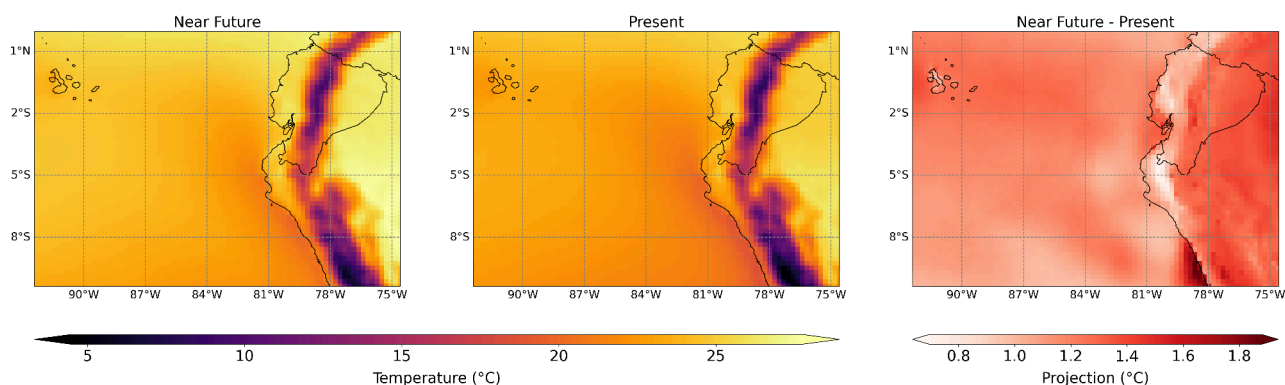


Figure 3.20: Near-surface air temperature for the near future (2021-2050) and present period (1991-2020) with their respective projection. The left panel shows the mean temperature for the near-future period, indicating higher temperatures compared to the present period shown in the middle panel. The projection in the right panel highlights an overall increase in temperature, with the most pronounced warming observed in the Amazon and Andean regions.

The analysis of near-surface air temperature projections for the near future (2021-2050) reveals significant warming across the region. The left panel of Figure 3.20 displays the mean temperature for the near-future period, showing higher temperatures compared to the present period (middle panel). The projection (right panel) indicates an overall increase in temperature, with the most pronounced warming observed in the Amazon and Andean regions. This increase in temperature is consistent with global climate change projections, which predict significant warming due to increased greenhouse gas concentrations⁷⁶.

The composite analysis for El Niño and La Niña events further highlights the expected changes in temperature patterns associated with these phenomena. The top row of Figure 3.21 shows the temperature composites for El Niño events in the near future and the present, along with their projection. The near-future El Niño composite indicates a noticeable increase in temperature compared to the present through all of continental Ecuador, but particularly in the Pacific Ocean. This warming trend during El Niño events is expected to exacerbate the already significant impacts of these events, such as increased heatwaves and altered precipitation patterns⁷⁴.

Similarly, the bottom row of Figure 3.21 presents La Niña composites. For La Niña events, the corrected model projections show a significant warming as well. The difference between the near-future and present composites (right panel) highlights an overall increase in temperature during La Niña events, although the warming is somewhat more intense compared to El Niño events, and very high

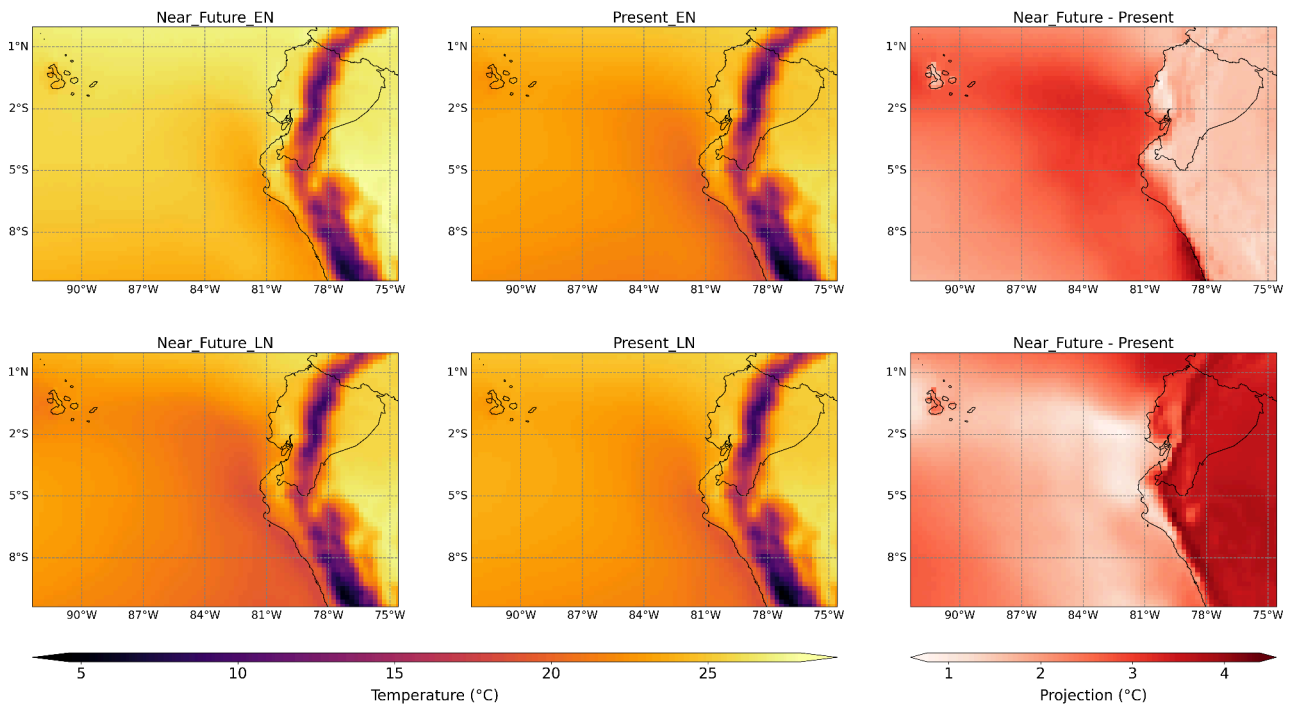


Figure 3.21: Composite near-surface air temperature for El Niño and La Niña events in the near future (2021-2050) compared to the present period (1991-2020). The top row shows El Niño events, indicating a noticeable increase in temperature in the near future, particularly over the Pacific Ocean. The bottom row presents La Niña events, with a significant warming observed in the near future, especially in the Andean region.

along the Andean region. This trend suggests a future climate scenario where even traditionally cooler La Niña periods will experience higher temperatures than currently observed, potentially altering the expected climate impacts of La Niña events⁶⁹.

It is also important to mention that the bias we applied to future temperature data helped to significantly increase confidence in climate projections, even though this variable did not show major improvements during validation as is the case for precipitation. Using corrected data for future projection observations helps us avoid systematic errors that could alter the results in some way. On the other hand, the observed warming trends for El Niño and La Niña events suggest an urgent need to prepare for a warmer climate, which could result in more severe and frequent extreme weather events. These projections are consistent with other studies that anticipate an increase in the frequency and intensity of extreme weather events due to global warming^{76,74}.

3.4.2 Total Precipitation

The total precipitation projections for the near future (2021-2050) show significant changes when compared to the present period (1991-2020). The left panel of Figure 3.22 presents the mean precipitation

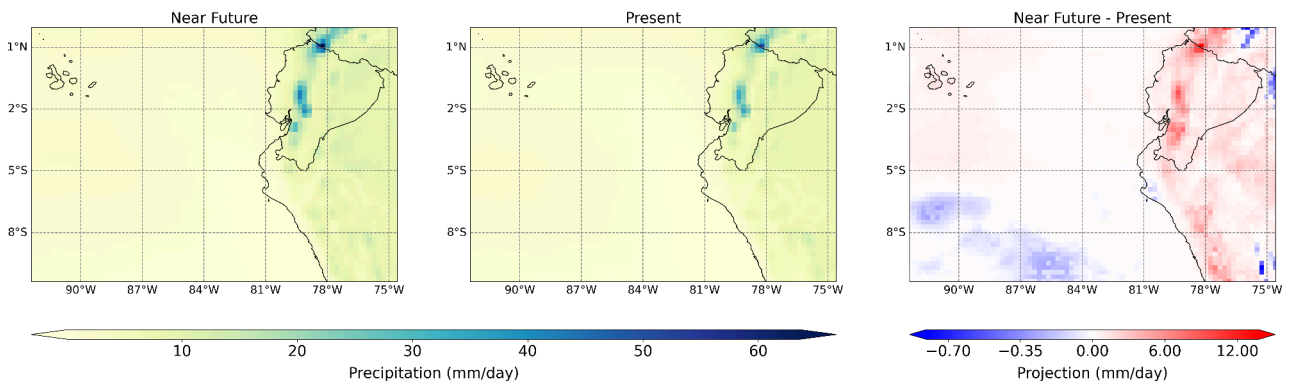


Figure 3.22: Total precipitation for the near future (2021-2050) and present period (1991-2020) with their respective projections. The left panel shows the mean precipitation for the near-future period, indicating changes in precipitation patterns across the region compared to the present period shown in the middle panel. The projection in the right panel highlights areas of increased precipitation, particularly in the coastal and Andean regions.

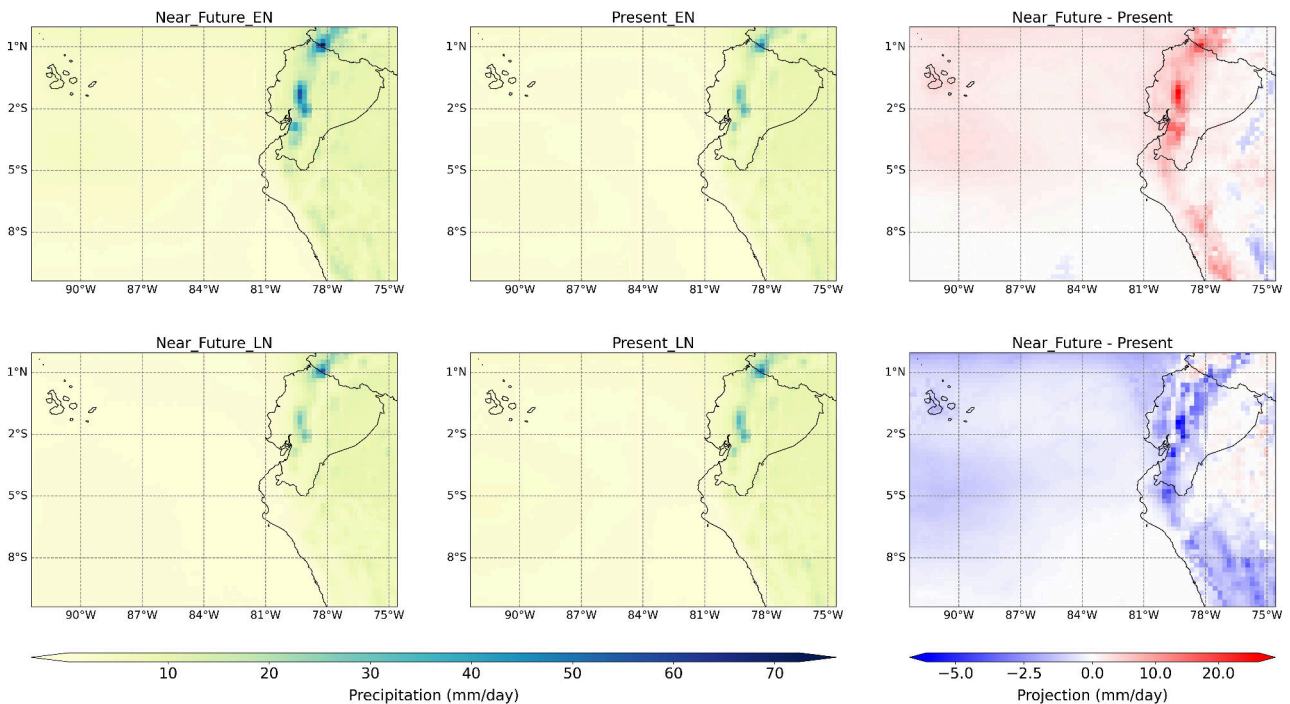


Figure 3.23: Composite total precipitation for El Niño and La Niña events in the near future (2021-2050) compared to the present period (1991-2020). The top row shows El Niño events, indicating a significant increase in precipitation in the near future, particularly along the Pacific coast and parts of the Andean regions. The bottom row presents La Niña events, with a noticeable decrease in precipitation in the near future, especially in the Pacific coast and the Andean region.

for the near-future period, revealing changes in precipitation patterns across the region. The middle panel displays the mean precipitation for the present period, serving as a baseline for comparison. The right panel highlights the differences between the two periods, indicating areas of increased and

decreased precipitation.

The analysis indicates that the coastal regions and parts of the Andean regions will experience increased precipitation in the near future, as indicated by the red areas in the projection map. This spatial variability in precipitation changes aligns with broader climate projections, which suggest that climate change will lead to more extreme weather patterns, including changes in precipitation intensity and distribution⁷⁶.

The composite analysis for El Niño and La Niña events provides further insights into how these precipitation patterns are expected to change during specific ENSO events. The top row of Figure 3.23 shows the precipitation composites for El Niño events in the near future and the present, along with their projections. During El Niño events, the near-future composite indicates a significant increase in precipitation in the northern coastal regions and parts of the Andean regions compared to the present. This increase is consistent with the enhanced convective activity and higher rainfall typically associated with El Niño events⁷⁴.

In contrast, the bottom row of Figure 3.23 presents La Niña composites. For La Niña events, the corrected model projections show a decrease in precipitation through Continental Ecuador, particularly for the Pacific coast and the Andean region. The difference between the near-future and present composites highlights a more pronounced drying trend in these regions during La Niña events, which could exacerbate drought conditions and impact water availability⁶⁹.

Overall, the bias correction we applied to the precipitation data greatly improved the accuracy of the projections, ensuring that near-future precipitation estimates are more reliable and in line with previously observed climate dynamics for ENSO events. Furthermore, these projections are also consistent with some studies indicating an increase in the frequency and intensity of extreme weather events as a result of global warming⁷⁶.

Chapter 4

Conclusions

This study aims to understand the impact of the El Niño-Southern Oscillation (ENSO) on inter-annual climate variations in Ecuador by using the Regional Climate Modeling System RegCM5 (version 5.0.0). High-resolution simulations were conducted, encompassing the complex topography of Ecuador and the Niño 1+2 region (Figure 3.19). The RegCM5 model, with its advanced MOLOCH non-hydrostatic dynamical core and various physics parameterizations, was driven by boundary conditions from the HadGEM2-ES General Circulation Model under the RCP8.5 scenario. The outputs from our numerical models for near-surface air temperature, total precipitation, and other climatic variables were validated against ERA5 reanalysis data. Bias correction using Quantile Delta Mapping (QDM) was applied to improve the accuracy of projections. ENSO events were identified using SST anomalies in the Niño 1+2 region, and future projections (2021-2050) were analyzed for changes in temperature and precipitation patterns during El Niño and La Niña events. This methodological approach ensured detailed and reliable future climate projections, essential for understanding and mitigating ENSO impacts on regional climate patterns in Ecuador. Our conclusions are listed below:

(i) On The Model Validation

The comparison of the RegCM5 model against ERA5 reanalysis data for the years 1991-2020 provides valuable insights into the performance of the model in simulating various climatic variables in Ecuador. The RegCM5 model successfully captures the spatial variability of near-surface air temperature across the country, as evidenced by high Willmott Index and Pearson Correlation values, which suggest strong alignment with the ERA5 data. Nonetheless, the model shows a tendency to overestimate temperatures, particularly in coastal regions and the Andes highlands. The model performs well during El Niño events, but it shows significant discrepancies during La Niña events, where it tends to overestimate temperatures. Precipitation modeling presents a greater challenge, with the RegCM5 model showing high errors and low correlation with the ERA5 data. The model tends to overestimate precipitation in the central Andean region and underestimate it along the coast and Amazon basin. These discrepancies are

more pronounced during El Niño and La Niña events, highlighting the difficulty of the model in accurately simulating precipitation under extreme climatic conditions. These errors are consistent with findings from previous studies, emphasizing the inherent challenges in precipitation modeling due to complex geographical and topographical influences. The discrepancies in wind divergence at 10m and 100m and relative humidity simulations are closely related to the performance of the model in simulating precipitation. Errors in wind divergence affect the vertical motion of air, which is crucial for cloud formation and precipitation. For instance, overestimations of wind divergence in coastal regions and underestimations in the Andean regions lead to incorrect precipitation estimates, as reflected in the precipitation analysis. Similarly, regions where the model overestimates relative humidity, such as the Andes, tend to show higher simulated precipitation amounts. Conversely, underestimations of relative humidity in coastal regions correlate with lower simulated precipitation.

(ii) *On The Bias Correction*

The bias correction applied to the RegCM5 model has been demonstrated to significantly improve the accuracy of both near-surface air temperature and total precipitation for the period 2011-2020. For near-surface air temperature, the corrected model markedly reduced the systematic warm bias that was prevalent in the original model, particularly in the coastal region. Notably, while the corrected model shows slight increases in MAE during El Niño events, it still achieves an overall reduction in bias and error magnitudes for La Niña events, making the temperature projections for the model more reliable for La Niña events. Similarly, the bias correction significantly improved the precipitation projections. The corrected model effectively mitigated the systematic overestimations observed in the original model, especially during the wet season and ENSO-related events. The error metrics for precipitation indicate dramatic reductions in MAE and RMSE, along with increased correlation coefficients and Willmott Index values, underscoring the improved performance of the model post-correction. The corrected model now aligns more closely with the ERA5 data, particularly during the ENSO events, providing a more accurate representation of this phenomenon.

(iii) *On the identification of El Niño and La Niña events*

Using the method proposed in this work to identify future ENSO events in the El Niño 1+2 region, we have indicated a similar count for the present period. The (1991-2020), ONI, used as a reference, gives a total of 19 events, the ERA5 data identified 25 events, and the bias-corrected RegCM5_QDM model produced 23 events. Although the ENSO events in this region produced by the model do not match the observations in time, this does not represent a drawback since the evolution of the variables of the regional model is forced by a global model and the objective is to observe the dynamics of the ENSO over the long term. After identifying the number of events for the near future, the model results in an increase in the frequency of El Niño events

and a decrease in La Niña events. The method may be used to help in the forecasting of future phenomena that might be associated with ENSO and Ecuador's vulnerable areas.

(iv) On the near-future projections

Regarding surface air temperature, the warming trend is very noticeable across the domain, particularly for coastal and Andean regions. During El Niño and La Niña events, this trend increases significantly in both cases, suggesting that even typically colder periods will experience elevated temperatures. These results agree with broader climate change projections that predict an increase in temperatures due to high concentrations of greenhouse gases. Regarding precipitation, our results suggest an increase in precipitation for coastal and Andean regions, which increases in intensity during El Niño events. Contrary to this, during La Niña events, these same regions will experience a considerable decrease in precipitation, which fits with the dynamic behavior of this variable during ENSO events.

While this study has provided valuable insights, some limitations need to be addressed. One significant limitation is that our RegCM5 simulation is not coupled with an ocean model, which could enhance the precision of identifying El Niño and La Niña events, and allow us to look deeper in the relevant region EL Niño 1+2. Coupled ocean-atmosphere models are more effective in simulating ENSO dynamics because they account for the feedback mechanisms between the ocean and the atmosphere, improving the accuracy of SST predictions¹³. The reliance on reanalysis data, like ERA5, also poses limitations due to its inherent biases and lack of in-situ data comparison. Reanalysis data are derived from a combination of model outputs and observations, which can introduce biases and uncertainties, particularly in regions with sparse observational data⁷⁷. Therefore, using in-situ data instead of reanalyzed data can help improve not only the accuracy but also the confidence in future climate projections. Future studies should incorporate comparisons with in-situ data to further refine model data. On the other hand, only one general circulation model was used in this research, so it would be interesting to explore whether other models can improve the identification of ENSO events or are even more effective in simulating climate variables for this region. Different GCMs have varying strengths and weaknesses in representing regional climate dynamics, so evaluating multiple models can help identify the most reliable ones for a specific region⁷⁸. Examples of GCMs that could be evaluated include the Community Earth System Model (CESM), the European Centre for Medium-Range Weather Forecasts (ECMWF), and the Max Planck Institute Earth System Model (MPI-ESM)⁷⁹. Implementing bias correction using in-situ data could offer significant benefits and further improve the model's accuracy. This comprehensive approach will enhance our understanding of ENSO impacts and improve the reliability of future climate projections.

Bibliography

- [1] Hoyer, S.; Hamman, J. xarray: ND labeled arrays and datasets in Python. *Journal of Open Research Software* **2017**, *5*, 10–10.
- [2] Hunter, J.; Dale, D. The matplotlib user's guide. *Matplotlib 0.90. 0 user's guide* **2007**,
- [3] May, R. M.; Goebbert, K. H.; Thielen, J. E.; Leeman, J. R.; Camron, M. D.; Bruick, Z.; Bruning, E. C.; Manser, R. P.; Arms, S. C.; Marsh, P. T. MetPy: A meteorological Python library for data analysis and visualization. *Bulletin of the American Meteorological Society* **2022**, *103*, E2273–E2284.
- [4] McPhaden, M. J.; Santoso, A.; Cai, W. Introduction to El Niño Southern Oscillation in a changing climate. *El Niño Southern Oscillation in a changing climate* **2020**, 1–19.
- [5] Ambrizzi, T.; Reboita, M. S.; da Rocha, R. P.; Llopart, M. The state of the art and fundamental aspects of regional climate modeling in South America. *Annals of the new york academy of sciences* **2019**, *1436*, 98–120.
- [6] Cai, W.; Santoso, A.; Collins, M.; Dewitte, B.; Karamperidou, C.; Kug, J.-S.; Lengaigne, M.; McPhaden, M. J.; Stuecker, M. F.; Taschetto, A. S. Changing El Niño-Southern oscillation in a warming climate. *Nature Reviews Earth & Environment* **2021**, *2*, 628–644.
- [7] Okumura, Y. M.; Deser, C. Asymmetry in the duration of El Niño and La Niña. *Journal of Climate* **2010**, *23*, 5826–5843.
- [8] Trenberth, K. E. The definition of el nino. *Bulletin of the American Meteorological Society* **1997**, *78*, 2771–2778.
- [9] McPhaden, M. J.; Zebiak, S. E.; Glantz, M. H. ENSO as an integrating concept in earth science. *science* **2006**, *314*, 1740–1745.
- [10] Trenberth, K. E. ENSO in the global climate system. *El Niño Southern Oscillation in a Changing Climate* **2020**, 21–37.

- [11] Santoso, A.; Hendon, H.; Watkins, A.; Power, S.; Dommenges, D.; England, M. H.; Frankcombe, L.; Holbrook, N. J.; Holmes, R.; Hope, P. Dynamics and predictability of El Niño–Southern Oscillation: an Australian perspective on progress and challenges. *Bulletin of the American Meteorological Society* **2019**, *100*, 403–420.
- [12] Capotondi, A.; Wittenberg, A. T.; Newman, M.; Di Lorenzo, E.; Yu, J.-Y.; Braconnot, P.; Cole, J.; Dewitte, B.; Giese, B.; Guilyardi, E. Understanding ENSO diversity. *Bulletin of the American Meteorological Society* **2015**, *96*, 921–938.
- [13] Zebiak, S. E.; Cane, M. A. A model el niñ–southern oscillation. *Monthly Weather Review* **1987**, *115*, 2262–2278.
- [14] Chakravorty, S.; Perez, R. C.; Anderson, B. T.; Larson, S. M.; Giese, B. S.; Pivotti, V. Ocean dynamics are key to extratropical forcing of El Niño. *Journal of Climate* **2021**, *34*, 8739–8753.
- [15] Clarke, A. J. *An introduction to the dynamics of El Niño and the Southern Oscillation*; Elsevier, 2008.
- [16] Cai, W.; McPhaden, M. J.; Grimm, A. M.; Rodrigues, R. R.; Taschetto, A. S.; Garreaud, R. D.; Dewitte, B.; Poveda, G.; Ham, Y.-G.; Santoso, A. Climate impacts of the El Niño–southern oscillation on South America. *Nature Reviews Earth & Environment* **2020**, *1*, 215–231.
- [17] Goddard, L.; Gershunov, A. Impact of El Niño on weather and climate extremes. *El Niño Southern Oscillation in a changing climate* **2020**, 361–375.
- [18] Garreaud, R. D.; Vuille, M.; Compagnucci, R.; Marengo, J. Present-day south american climate. *Palaeogeography, Palaeoclimatology, Palaeoecology* **2009**, *281*, 180–195.
- [19] Grimm, A. M. Interannual climate variability in South America: impacts on seasonal precipitation, extreme events, and possible effects of climate change. *Stochastic Environmental Research and Risk Assessment* **2011**, *25*, 537–554.
- [20] Echevin, V.; Colas, F.; Espinoza-Morriberon, D.; Vasquez, L.; Anculle, T.; Gutierrez, D. Forcings and evolution of the 2017 coastal El Niño off Northern Peru and Ecuador. *Frontiers in Marine Science* **2018**, *5*, 367.
- [21] Campozano, L.; Robaina, L.; Samaniego, E. The Pacific decadal oscillation modulates the relation of ENSO with the rainfall variability in coast of Ecuador. *International Journal of Climatology* **2020**, *40*, 5801–5812.
- [22] Bendix, A.; Bendix, J. Heavy rainfall episodes in Ecuador during El Niño events and associated regional atmospheric circulation and SST patterns. *Advances in Geosciences* **2006**, *6*, 43–49.

- [23] Recalde-Coronel, G. C.; Barnston, A. G.; Muñoz, Á. G. Predictability of December–April rainfall in coastal and Andean Ecuador. *Journal of Applied Meteorology and Climatology* **2014**, *53*, 1471–1493.
- [24] Vuille, M.; Bradley, R. S.; Keimig, F. Climate variability in the Andes of Ecuador and its relation to tropical Pacific and Atlantic sea surface temperature anomalies. *Journal of climate* **2000**, *13*, 2520–2535.
- [25] Vicente-Serrano, S. M.; Aguilar, E.; Martínez, R.; Martín-Hernández, N.; Azorin-Molina, C.; Sánchez-Lorenzo, A.; El Kenawy, A.; Tomás-Burguera, M.; Moran-Tejeda, E.; López-Moreno, J. I. The complex influence of ENSO on droughts in Ecuador. *Climate Dynamics* **2017**, *48*, 405–427.
- [26] Campozano, L.; Vázquez-Patiño, A.; Tenelanda, D.; Feyen, J.; Samaniego, E.; Sánchez, E. Evaluating extreme climate indices from CMIP3&5 global climate models and reanalysis data sets: a case study for present climate in the Andes of Ecuador. *International Journal of Climatology* **2017**, *37*, 363–379.
- [27] Ng, B.; Cai, W.; Cowan, T.; Bi, D. Impacts of low-frequency internal climate variability and greenhouse warming on El Niño–Southern Oscillation. *Journal of Climate* **2021**, *34*, 2205–2218.
- [28] Collins, M.; An, S.-I.; Cai, W.; Ganachaud, A.; Guilyardi, E.; Jin, F.-F.; Jochum, M.; Lengaigne, M.; Power, S.; Timmermann, A. The impact of global warming on the tropical Pacific Ocean and El Niño. *Nature Geoscience* **2010**, *3*, 391–397.
- [29] Pareja-Quispe, D.; Franchito, S. H.; Fernandez, J. P. R. Assessment of the RegCM4 performance in simulating the surface radiation budget and hydrologic balance variables in South America. *Earth Systems and Environment* **2021**, *5*, 499–518.
- [30] Portele, T. C.; Laux, P.; Lorenz, C.; Janner, A.; Horna, N.; Fersch, B.; Iza, M.; Kunstmann, H. Ensemble-tailored pattern analysis of high-resolution dynamically downscaled precipitation fields: example for climate sensitive regions of South America. *Frontiers in Earth Science* **2021**, *9*, 669427.
- [31] Chimborazo, O.; Vuille, M. Present-day climate and projected future temperature and precipitation changes in Ecuador. *Theoretical and Applied Climatology* **2021**, *143*, 1581–1597.
- [32] Chimborazo, O. *Projected Changes in Climate, Elevation-dependent Warming, and Extreme Events over Continental Ecuador for the Period 2041-2070*; State University of New York at Albany, 2018.

- [33] Sangelantoni, L.; Ricchi, A.; Ferretti, R.; Redaelli, G. Dynamical downscaling in seasonal climate forecasts: Comparison between RegCM-and WRF-based approaches. *Atmosphere* **2021**, *12*, 757.
- [34] Corrêa, C. S.; de Queiroz, A. P.; Camillo, G. L. Study of the convergence of low cloudiness by the effect of ocean breeze using the regional climate model: Estudo da convergência de nuvem em baixos níveis pelo efeito da brisa oceanica usando um modelo de clima regional. *Latin American Journal of Development* **2022**, *4*, 880–893.
- [35] Giorgi, F.; Coppola, E.; Giuliani, G.; Ciarlo, J. M.; Pichelli, E.; Nogherotto, R.; Raffaele, F.; Malguzzi, P.; Davolio, S.; Stocchi, P. The Fifth Generation Regional Climate Modeling System, RegCM5: Description and Illustrative Examples at Parameterized Convection and Convection-Permitting Resolutions. *Journal of Geophysical Research: Atmospheres* **2023**, *128*, e2022JD038199.
- [36] Campozano, L.; Trachte, K.; Célleri, R.; Samaniego, E.; Bendix, J.; Albuja, C.; Mejia, J. F. Climatology and teleconnections of mesoscale convective systems in an Andean basin in southern Ecuador: the case of the Paute basin. *Advances in Meteorology* **2018**, *2018*, 4259191.
- [37] Collins, W.; Bellouin, N.; Doutriaux-Boucher, M.; Gedney, N.; Halloran, P.; Hinton, T.; Hughes, J.; Jones, C.; Joshi, M.; Liddicoat, S. Development and evaluation of an Earth-System model–HadGEM2. *Geoscientific Model Development* **2011**, *4*, 1051–1075.
- [38] Jones, C.; Hughes, J.; Bellouin, N.; Hardiman, S.; Jones, G.; Knight, J.; Liddicoat, S.; O’connor, F.; Andres, R. J.; Bell, C. The HadGEM2-ES implementation of CMIP5 centennial simulations. *Geoscientific Model Development* **2011**, *4*, 543–570.
- [39] Da Rocha, R. P.; Reboita, M. S.; Dutra, L. M. M.; Llopart, M. P.; Coppola, E. Interannual variability associated with ENSO: present and future climate projections of RegCM4 for South America-CORDEX domain. *Climatic Change* **2014**, *125*, 95–109.
- [40] Van Vuuren, D. P.; Edmonds, J.; Kainuma, M.; Riahi, K.; Thomson, A.; Hibbard, K.; Hurtt, G. C.; Kram, T.; Krey, V.; Lamarque, J.-F. The representative concentration pathways: an overview. *Climatic change* **2011**, *109*, 5–31.
- [41] Nayak, S.; Mandal, M.; Maity, S. RegCM4 simulation with AVHRR land use data towards temperature and precipitation climatology over Indian region. *Atmospheric research* **2018**, *214*, 163–173.
- [42] Giorgi, F.; Mearns, L. O. Introduction to special section: Regional climate modeling revisited. 1999.

- [43] Holton, J. R.; Hakim, G. J. *An introduction to dynamic meteorology*; Academic press, 2013; Vol. 88.
- [44] Kiehl, J.; Schneider, T.; Rasch, P.; Barth, M.; Wong, J. Radiative forcing due to sulfate aerosols from simulations with the National Center for Atmospheric Research Community Climate Model, Version 3. *Journal of Geophysical Research: Atmospheres* **2000**, *105*, 1441–1457.
- [45] Holtslag, A.; Ek, M. Simulation of surface fluxes and boundary layer development over the pine forest in HAPEX-MOBILHY. *Journal of Applied Meteorology and Climatology* **1996**, *35*, 202–213.
- [46] Grell, G. A. Prognostic evaluation of assumptions used by cumulus parameterizations. *Monthly weather review* **1993**, *121*, 764–787.
- [47] Emanuel, K. A.; Živković-Rothman, M. Development and evaluation of a convection scheme for use in climate models. *Journal of the Atmospheric Sciences* **1999**, *56*, 1766–1782.
- [48] Reboita, M. S.; Fernandez, J. P. R.; Llopart, M. P.; da Rocha, R. P.; Pampuch, L. A.; Cruz, F. T. Assessment of RegCM4. 3 over the CORDEX South America domain: sensitivity analysis for physical parameterization schemes. *Climate Research* **2014**, *60*, 215–234.
- [49] Oleson, K. W.; Lawrence, D. M.; Bonan, G. B.; Drewniak, B.; Huang, M.; Koven, C. D.; Levis, S.; Li, F.; Riley, W. J.; Subin, Z. M. Technical description of version 4.0 of the Community Land Model (CLM). *NCAR Tech. Note NCAR/TN-478+ STR* **2010**, *257*, 1–257.
- [50] Pal, J. S.; Small, E. E.; Eltahir, E. A. Simulation of regional-scale water and energy budgets: Representation of subgrid cloud and precipitation processes within RegCM. *Journal of Geophysical Research: Atmospheres* **2000**, *105*, 29579–29594.
- [51] Zeng, X.; Zhao, M.; Dickinson, R. E. Intercomparison of bulk aerodynamic algorithms for the computation of sea surface fluxes using TOGA COARE and TAO data. *Journal of Climate* **1998**, *11*, 2628–2644.
- [52] Hersbach, H.; Bell, B.; Berrisford, P.; Hirahara, S.; Horányi, A.; Muñoz-Sabater, J.; Nicolas, J.; Peubey, C.; Radu, R.; Schepers, D. The ERA5 global reanalysis. *Quarterly Journal of the Royal Meteorological Society* **2020**, *146*, 1999–2049.
- [53] Wilks, D. S.; Wilby, R. L. The weather generation game: a review of stochastic weather models. *Progress in physical geography* **1999**, *23*, 329–357.
- [54] Jones, P. D.; Moberg, A. Hemispheric and large-scale surface air temperature variations: An extensive revision and an update to 2001. *Journal of climate* **2003**, *16*, 206–223.

- [55] Trenberth, K. E.; Dai, A.; Rasmussen, R. M.; Parsons, D. B. The changing character of precipitation. *Bulletin of the American Meteorological Society* **2003**, *84*, 1205–1218.
- [56] Bolton, D. The computation of equivalent potential temperature. *Monthly weather review* **1980**, *108*, 1046–1053.
- [57] Rogers, R.; Yau, M. A short course in cloud physics. *Bull. Amer. Meteor. Soc* **1996**, *45*, 619.
- [58] Willmott, C. J.; Matsuura, K. Advantages of the mean absolute error (MAE) over the root mean square error (RMSE) in assessing average model performance. *Climate research* **2005**, *30*, 79–82.
- [59] Chai, T.; Draxler, R. R. Root mean square error (RMSE) or mean absolute error (MAE)?—Arguments against avoiding RMSE in the literature. *Geoscientific model development* **2014**, *7*, 1247–1250.
- [60] Wilks, D. S. *Statistical methods in the atmospheric sciences*; Academic press, 2011.
- [61] Taylor, K. E. Summarizing multiple aspects of model performance in a single diagram. *Journal of geophysical research: atmospheres* **2001**, *106*, 7183–7192.
- [62] Willmott, C. J. On the validation of models. *Physical geography* **1981**, *2*, 184–194.
- [63] Teutschbein, C.; Seibert, J. Bias correction of regional climate model simulations for hydrological climate-change impact studies: Review and evaluation of different methods. *Journal of hydrology* **2012**, *456*, 12–29.
- [64] Cannon, A. J.; Sobie, S. R.; Murdock, T. Q. Bias correction of GCM precipitation by quantile mapping: how well do methods preserve changes in quantiles and extremes? *Journal of Climate* **2015**, *28*, 6938–6959.
- [65] Tong, Y.; Gao, X.; Han, Z.; Xu, Y.; Xu, Y.; Giorgi, F. Bias correction of temperature and precipitation over China for RCM simulations using the QM and QDM methods. *Climate Dynamics* **2021**, *57*, 1425–1443.
- [66] Garreaud, R. D.; Alvarez-Garreton, C.; Barichivich, J.; Boisier, J. P.; Christie, D.; Galleguillos, M.; LeQuesne, C.; McPhee, J.; Zambrano-Bigiarini, M. The 2010–2015 megadrought in central Chile: impacts on regional hydroclimate and vegetation. *Hydrology and earth system sciences* **2017**, *21*, 6307–6327.
- [67] Ramírez, I. J.; Briones, F. Understanding the El Niño costero of 2017: The definition problem and challenges of climate forecasting and disaster responses. *International Journal of Disaster Risk Science* **2017**, *8*, 489–492.

- [68] Gloor, M.; Brienen, R. J.; Galbraith, D.; Feldpausch, T. R.; Schöngart, J.; Guyot, J.-L.; Espinoza, J. C.; Lloyd, J.; Phillips, O. L. Intensification of the Amazon hydrological cycle over the last two decades. *Geophysical Research Letters* **2013**, *40*, 1729–1733.
- [69] Cai, W.; Wang, G.; Santoso, A.; McPhaden, M. J.; Wu, L.; Jin, F.-F.; Timmermann, A.; Collins, M.; Vecchi, G.; Lengaigne, M. Increased frequency of extreme La Niña events under greenhouse warming. *Nature Climate Change* **2015**, *5*, 132–137.
- [70] Rauscher, S. A.; Giorgi, F.; Diffenbaugh, N. S.; Seth, A. Extension and intensification of the Meso-American mid-summer drought in the twenty-first century. *Climate Dynamics* **2008**, *31*, 551–571.
- [71] Maraun, D.; Wetterhall, F.; Ireson, A.; Chandler, R.; Kendon, E.; Widmann, M.; Brienen, S.; Rust, H.; Sauter, T.; Themeßl, M. Precipitation downscaling under climate change: Recent developments to bridge the gap between dynamical models and the end user. *Reviews of geophysics* **2010**, *48*.
- [72] Yang, K.; Guyennon, N.; Ouyang, L.; Tian, L.; Tartari, G.; Salerno, F. Impact of summer monsoon on the elevation-dependence of meteorological variables in the south of central Himalaya. *International Journal of Climatology* **2018**, *38*, 1748–1759.
- [73] Salby, M. L. *Physics of the Atmosphere and Climate*; Cambridge University Press, 2012.
- [74] Cai, W.; Borlace, S.; Lengaigne, M.; Van Rensch, P.; Collins, M.; Vecchi, G.; Timmermann, A.; Santoso, A.; McPhaden, M. J.; Wu, L. Increasing frequency of extreme El Niño events due to greenhouse warming. *Nature climate change* **2014**, *4*, 111–116.
- [75] Timmermann, A.; An, S.-I.; Kug, J.-S.; Jin, F.-F.; Cai, W.; Capotondi, A.; Cobb, K. M.; Lengaigne, M.; McPhaden, M. J.; Stuecker, M. F. El Niño–southern oscillation complexity. *Nature* **2018**, *559*, 535–545.
- [76] Change, I. Climate change 2007: The physical science basis. *Agenda* **2007**, *6*, 333.
- [77] Bengtsson, L.; Hagemann, S.; Hodges, K. I. Can climate trends be calculated from reanalysis data? *Journal of Geophysical Research: Atmospheres* **2004**, *109*.
- [78] Flato, G.; Marotzke, J.; Abiodun, B.; Braconnot, P.; Chou, S. C.; Collins, W.; Cox, P.; Driouech, F.; Emori, S.; Eyring, V. *Climate change 2013: the physical science basis. Contribution of Working Group I to the Fifth Assessment Report of the Intergovernmental Panel on Climate Change*; Cambridge University Press, 2014; pp 741–866.

- [79] Eyring, V.; Bock, L.; Lauer, A.; Righi, M.; Schlund, M.; Andela, B.; Arnone, E.; Bellprat, O.; Brötz, B.; Caron, L.-P. Earth System Model Evaluation Tool (ESMValTool) v2. 0—an extended set of large-scale diagnostics for quasi-operational and comprehensive evaluation of Earth system models in CMIP. *Geoscientific Model Development* **2020**, *13*, 3383–3438.